Modeling of Positive-Displacement Dispensing Process

A Thesis Submitted to the College of

Graduate Studies and Research

in Partial Fulfillment of the Requirements

for the Degree of Master of Science

in the Department of Mechanical Engineering

University of Saskatchewan

Saskatoon

By

Jun Kai

PERMISSION TO USE

In presenting this thesis in partial fulfillment of the requirements for a Postgraduate degree from the University of Saskatchewan, I agree that the Libraries of this University may make it freely available for inspection. I further agree that permission for copying of this thesis in any manner, in whole or in part, for scholarly purposes may be granted by the professor or professors who supervised my thesis work or, in their absence, by the Head of the Department or the Dean of the College in which my thesis work was done. It is understood that any copying or publication or use of this thesis or parts thereof for financial gain shall not be allowed without my written permission. It is also understood that due recognition shall be given to me and to the University of Saskatchewan in any scholarly use which may be made of any material in my thesis.

Requests for permission to copy or to make other use of material in this thesis in whole or part should be addressed to:

Head of the Department of Mechanical Engineering

University of Saskatchewan

Saskatoon, Saskatchewan, S7N 5A9

ABSTRACT

Fluid dispensing is a method by which fluid materials are delivered to the targeted boards in a controlled manner and has been extensively applied in various packaging processes in the electronics assembly industry. In these processes, the flow rate of the fluid dispensed and/or the fluid amount transferred onto a board are two important performance indexes. Due to the involvement of the compressibility and non-Newtonian behaviour of the fluid being dispensed, modeling the fluid dispensing process has proven to be a challenging task. This thesis presents a study on the modeling of the positive displacement dispensing process, in which the linear displacement of a piston is used to dispense fluid. Also, this thesis presents an evaluation of different designs of the fluid dispensing system based on the axiomatic design principles.

At first, the characterization of the flow behaviour of fluids used in the electronic packaging industry is addressed. Based on the previous experiments conducted in the author's lab, a 3-parameter Carreau model for the fluid Hysol FP4451 is derived for use in the present study. Then, taking into account fluid compressibility and flow behaviour, a model is developed to represent the dynamics of the flow rate of the fluid dispensed. The resulting model suggests that the dynamics of the flow rate in the positive displacement dispensing process is equivalent to that of a second order system. Based on the model developed, the influences of the fluid compressibility and the process parameters such as the dispensing time and needle temperature are investigated by simulations.

In the positive dispensing process, it is noticed that the fluid amount dispensed out of needle is different from the fluid amount finally transferred to the board, if the fluid amount dispensed is very small. This difference is considered one major problem affecting dispensing performance. In order to determine the fluid amount transferred to the board, a 3-step method is developed in the present study, based on existing theories of liquid bridges and Laplace's equation. Simulations are conducted based on the developed method to study the influence of surface tension and initial fluid amount on the final fluid amount transferred onto the board.

Finally, this thesis presents a new approach to evaluate and compare different designs of the fluid dispensing system, namely air-pressure, rotary-crew, and positive-displacement. In this approach, the axiomatic design principles, i.e., the Independence Axiom and the Information Axiom, are employed. This approach can be used not only to evaluate existing dispensing systems, but also to design new dispensing systems.

ACKNOWLEDGMENTS

First, I would like to express my heartfelt gratitude to my supervisor, Prof. Dr. Daniel X.B. Chen for his generous guidance, academic criticism, suggestions, and continuous encouragement which have made the completion of this work possible.

Second, I would like to extend the appreciation to those members of my Advisory Committee, Prof. Chris Zhang and Prof. James Bugg for their academic examinations and advice during the study.

The financial support from Natural Science and Engineering Research Council (NSERC) of Canada and Dept. of Mechanical Engineering of the University of Saskatchewan (through the scholarship) is acknowledged.

I would also like to thank all my friends and classmates for their discussion, advice and friendship. Special thanks go to Dr. Monte Keene Pishny-Floyd and his wife Mrs. Annette Pishny-Floyd for their kindness, hospitalities, and home-feeling treatment when I lived in their home.

Finally, I wish to thank my parents and my dear wife, Chun Fu, for their consistent love, encouragement, and support.

TABLE OF CONTENTS

LIST OF TABLES

LIST OF FIGURES

NOMENCLATURE

$[A]$: Design matrix, dimensionless

A0 : Minimum section area along the bridge, m^2

A_{ij} : Element in the design matrix, dimensionless

A_o : Area of air flow passage of orifice, m^2

A_p : Piston cross-section area, m^2

A_n : Cross-section area of the needle, m^2

B : Fluid bulk modulus, Pa

$[B]$: Extra matrix, dimensionless

B_{ij} : Element in the extra matrix, dimensionless

c_1, c : Constant with the dimension of time, s

C : Syringe capacity, m^3

C_d : Discharge coefficient, dimensionless

C_m : Mass flow parameter, dimensionless

C_p : Coefficient associated with the pure pressure flow, dimensionless

C_ω : Coefficient associated with the pure drag flow, dimensionless

D_n : Needle inner diameter, m

D_p : Diameter of piston, m

DP_i: Design parameters, dimensionless

D_{sw} : Diameter of rotary screw, m

FR_i: Functional requirements, dimensionless

F_0: Force imposed on the top plate, N

$F_{d,p}$: Geometric form factors, dimensionless

F_{ex} : Total extensional force, N

F_z : Surface tension force in Z direction, N/m

F_σ : Surface tension force at $z = \Delta z$ circle, N/m

g: Gravity acceleration, 9.8 m/s^2

H : Distance between the thread root and syringe wall/channel depth, m

$h(z)$: Liquid bridge radius in the h, z coordinates, m

I : Information content, bit

k : Consistency index, $Pa \cdot s^n$

K : Coefficient associated the effect of temperature on viscosity (Pa·s)

l_a : Total length of syringe, m

L : Liquid bridge extended length, m

$L1$: Length from Z=0 to a section of the same radius $R0$, m

L_0 : Liquid bridge initial length, m

L_n : Needle length, m

L_c : Length of the fluid in down channel direction, m

L(t) : Instantaneous liquid bridge length, m

$L(t\_break)$: Breaking length, m

$\dot{m}$: Mass flow rate of air into the syringe through orifice, kg/s

$M(\Delta z)$: Fluid mass between the $z = 0$ and z = Δz sections

M : The fluid amount dispensed, kg

M_c : Magnitude of the manipulated parameter

$M\_(L1)$: Fluid mass from needle outlet to $L1$ section

n : Flow behaviour index, dimensionless

n_t : Number of parallel threads, dimensionless

P : Supplied air pressure in time-pressure dispensing, Pa

P_0 : Ambient pressure, Pa

P_1 : Pressure at auger input, Pa

P_2 : Pressure at auger output & needle input, Pa

P_{FR} : Probability of success, dimensionless

P_g : Pressure in needle hub, Pa

P_e : Pressure at needle outlet, Pa

P_s : Fluid pressure at the syringe bottom, Pa

P_t : Fluid pressure at the syringe top, Pa

P' : Pressure on the convex side of the surface, Pa

P'' : Pressure on the concave side of the surface, Pa

$P\_z(0)$: Internal pressure in the middle point of needle outlet, Pa

Q : Flow rate of the fluid dispensed, m^3/s

Q_u : Steady-state flow rate under a unit pressure, m^3/s

r : Cross-section radius at $L(t)/2$ position, m

r_1, r_2 : Principal radii of curvature, m

$r(t)$: Liquid bridge radius at time t, m

R : Constant (J/kg/K)

R_0 : Initial radius of the liquid bridge, m

R_1, R_2 : Curvature radii, m

$R0$: Outside radius of the needle, m

$R_{mid}(t)$: liquid bridge mid-plane radius, m

t : Time, s

T : System temperature, ^oC

t_d : Time period of dispensing, s

T_c : Duration of the manipulated parameter, s

T_K : Coefficient associated the effect of temperature on viscosity, ^oC

T_R : Trouton ratio, Dimensionless

u : Average flow velocity of fluid in the needle, m/s

u_i : Change in FR due to the variation of primary DPs in uncoupled designs

V_p : Piston motion velocity, m/s

$\mathcal{V}_0$: Extension velocity, m/s

V_0 : Initial fluid volume in the syringe, m^3

V_a : Air volume in the syringe, m^3

V_f : Fluid volume in the syringe, m^3

V_L : Liquid bridge volume, m^3

W : Cross channel width, m

X : Position of piston in the syringe, m

$\dot{X}$: Piston movement speed, m/s

y : Coordinate, dimensionless

Z : Coordinate, dimensionless

γ : Ratio of the specific heats

$\dot{\gamma}$: Shear rate, s^{-1}

$\Delta(z)$: Step distance, m

ε_c : Critical extensional strain, dimensionless

ε_h : Henkey strain, dimensionless

$\dot{\varepsilon}$: Extension rate, dimensionless

$\dot{\varepsilon}_0$: Initial strain rate, s^{-1}

η : Fluid viscosity, Pa·s

η_0 : Asymptotic values of viscosity at very low shear rates, Pa.s

η_∞ : Asymptotic values of viscosity at very high shear rates, Pa.s

η_E : Extensional viscosity, Pa.s

η_s : Shear viscosity, Pa.s

$\eta_E^+(t,\dot{\varepsilon})$: Transient extensional viscosity, Pa.s

$\delta \mathrm{DP}_i$: Random variation in DP_i, dimensionless

μ : Fluid viscosity, Pa.s

ρ : Fluid density, kg/m^3

σ : Surface tension, N/m

τ : Shear stress, N/m^2

τ_0 : Yield stress, N/m^2

τ_{rr} : Stress in radial *R* direction, N/m^2

τ_w : Shear stress at the needle wall, N/m^2

τ_{zz} : Extension stress in *Z* direction, N/m^2

ϕ : Syringe lead angle, degree

φ : Contact angle, degree

$\chi \mathrm{FR}_i$: Extreme value of the random variation in FR_i

ω : Screw angular speed, rad/s

1. INTRODUCTION

1.1 Dispensing Applications

Fluid dispensing is a method by which fluid materials are delivered in a precisely controlled manner. It has been widely used in applications such as electronics assembly [Dixon *et al.* 1997, Ness and Lewis 1998, Wedekin 2001] and micro-electro-mechanical systems (MEMS) assembly [Lewis *et al.* 2003, Hsu 2004]. In these applications, minute volumes typically varying from microliters to nanoliters of fluids (e.g. epoxy, adhesive, encapsulant, hydrogel, etc.) must be delivered accurately. Generally, liquid dispensing applications can be classified into three categories: dam and filling, glob top, and under-filling, as shown in Figure 1.1

(a) (b) (c)

Figure 1.1 Dispensing applications
[Babiarz et al. 1999; www.shinetsu-encap-mat.jp]
(a) dam and filling; (b) glob-top process; and (c) under-filling

1.1.1 Dam and Filling

In the dam and filling process shown in Figure 1.1 (a), a die and wires between the die and substrate need to be enclosed in an encapsulation to protect them from

any environmental attacks. For this purpose, the dam and filling process includes two steps: first a high viscosity encapsulant is dispensed around the cavity edge or the die to form the dam, and then a lower viscosity encapsulant is dispensed to fill the space or cavity limited by the dam material. Both steps are critical to the ultimate shape height and flatness of the surface.

1.1.2 Glob Top

The Glob Top process is used to protect the die and interconnections without the need for a dam process. As a filling process, glob tops are used to the directly attach packages, such as chips on boards and tape carrier packages. In such applications, encapsulant is deposited on the top of components or dies, covering and protecting the interconnections. Because of the absence of the dam process, the control of dispensing material amount plays an important role in the final shape and packaging quality. The amount should be just enough to cover the selected encapsulation area, and not be excessive to contaminate other components on the Printed Circuit Board (PCB). The amount, therefore, needs to be controlled precisely in this application.

1.1.3 Underfilling Process

In electronics manufacturing, the component size has continuously became smaller for more efficient use of resources and also more convenient and consumer

friendly products. Examples that represent the trends are a silicon chip that once held hundreds of transistors now holds millions and palm-sized computers compared to warehouse sized computers forty years ago. As the chip size decreases and the number of I/Os (Input/Output) increases, it becomes difficult to apply the wire bond technology to the packaging. One solution is the use the flip-chip technology, as shown in Figure 1.2, in which a die is connected to the substrate by means of conductive bumps, which can be seen in Figure 1.3. In order to reduce the stress caused by the difference in the coefficient of thermal expansion (CTE) between the die and the substrate, the gap (typically 50 μm) [Wan 2004] between them must be filled by encapusulant. This process is called underfilling. Figure 1.3 shows schematically dispensing encapsulant for the underfilling process. The encapsulant is dispensed starting from one side of the die and then drawn by capillary forces to fill the gap between the chip and the substrate.

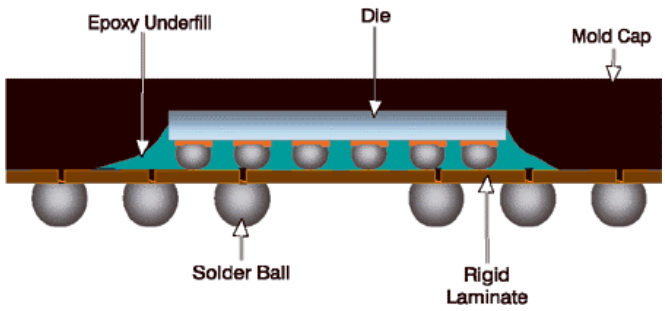

Figure 1.2 Flip-chip Cross-section [www.amkor.com]

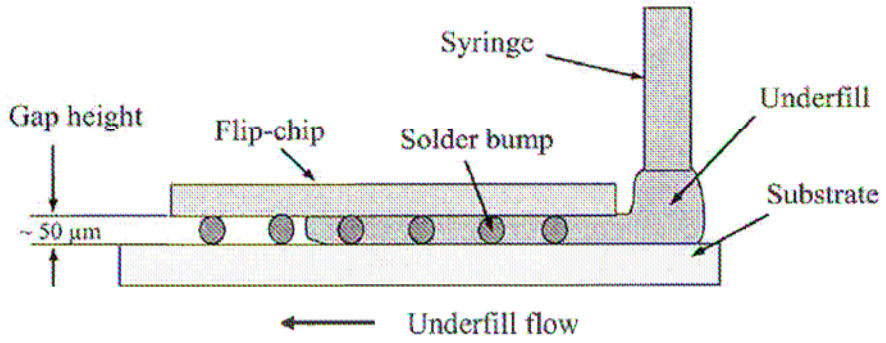

Figure 1.3 Dispensing for underfill process

One potential defect of the underfilling process is the voids formed between the die and substrate [Yang *et al.* 2003]. One possible reason for the defect is that the amount of dispensed underfilling encapsulant may be less than what is expected. This is particularly true for the cases where the underfilling gap is narrow, the solder bump diameter is small, and the number of bumps is huge. To alleviate this problem, the encapsulate amount dispensed must be well controlled.

From the above discussion, it is seen that precise dispensing is a key step in the electronics packaging industry. With decreasing in the component size, advances in dispensing technologies must be made accordingly in order to increase the final package quality. Taking surface mounting technology (SMT) as an example, when the component size decreases, so does the gap between the leads. It is therefore necessary for the size of the adhesive dot to decrease to the same degree to guarantee qualified packaging. Current technology can produce dots of surface mount adhesive of approximately 0.5 mm diameter and roughly 0.03-0.04 ml in volume. Due to the continuing trend of component scale reduction, it is expected

that dots in a 0.15-0.25 mm diameter range will be required [Quinones *et al.* 2003]. This leads to a need to model the dispensing process.

1.2 Fluid Dispensing Methods

A variety of fluid dispensing methods are now available for the aforementioned applications [Chen *et al.* 1999, Murch *et al.*1997, Babiarz 1999, Ness and Lewis 1997]. These approaches can be classified, in terms of driving mechanism, into three categories: time-pressure, rotary screw, and positive-displacement as shown in Figure 1.4.

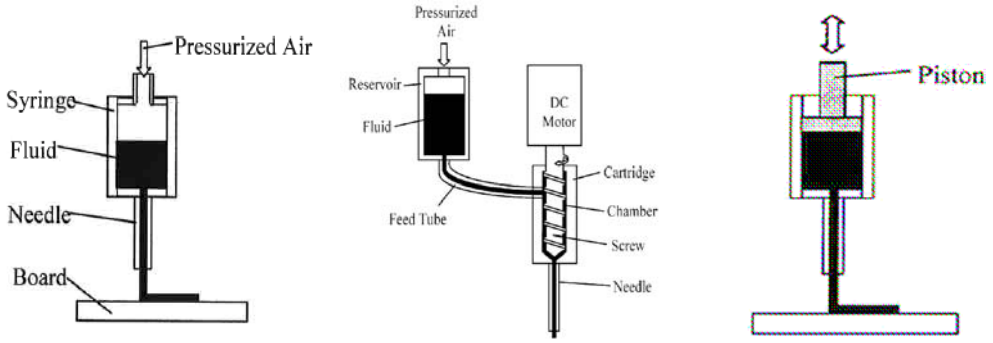

(a) Time-Pressure (b) Rotary-screw (c) Positive-displacement

Figure 1.4 Schematic diagrams of fluid dispensing methods

Figure 1.4(a) shows the time-pressure method. In this method, the fluid in the syringe is exposed to pressurized air during the dispensing cycle and forced out of the needle. Once the pressure is relieved, the dispensing process is stopped. To improve dispensing quality, some modifications have been made such as adding vacuum to prevent the material from dripping when the valve is idle, and varying the magnitude of air pressure according to the amount of material in the syringe.

Another way to control the fluid amount more precisely is using an additional shut-off valve at the end of the needle [Krieger and Behler 1998]. This valve controls the dispensing amount by opening or closing the passage to the needle. This method is especially valuable when dispensing encapsulant with low viscosity as it is able to eliminate unexpected dripping. Time-pressure dispensing has been most widely used due to its flexibility to different applications, simple operation and easy maintenance. However, the dispensed amount can be affected significantly by the flow behaviour of the fluid being dispensed and the air compressibility [Chen *et al*. 2000].

For viscous encapsulant materials, the most commonly used dispensing method is the rotary screw [Okada *et al.* 2004], as shown in Figure 1.4(b). The method employs a motor-driven auger to push fluid down to the bottom of the syringe. Due to the rotation of the auger, a high fluid pressure is produced at the bottom of the syringe; and under its action, the fluid in the needle is extruded out of the needle. Since the pressure built at the bottom causes an upward flow, this dispensing method is also sensitive to the fluid viscosity but is less dependent on it compared to time-pressure method [Babiarz 1999, Ness and Lewis 1997].

Positive-displacement is one of the most accurate methods currently available [Lewis and Ciardella 1999]. In this dispensing method, the linear movement of a piston is used to force the fluid out of the metering chamber, depositing the displaced amount of fluid through the outlet. The obvious advantage of the method

is that the fluid amount dispensed depends only on the linear movement of the piston. However, this is not valid for small volume of fluid [Chen and Kai 2004] due to the influence of the fluid compressibility. Compared to the time-pressure and rotary-screw methods, the positive-displacement method provides the most accurate flow rate of dispensing, but the cost is the highest of the three.

1.3 Review of Modeling of Dispensing Methods and Process

Modeling dispensing process has both theoretical and practical value. From the theoretical point of view, dispensing process modeling will improve the understanding of the influences of fluid behaviour, mechanical structure, as well as dispensing process parameters on the performance. From the practical point of view, an accurate model will benefit the process control by improving the dispensing performance, such as flow rate and/or fluid amount. The modeling of the three dispensing methods discussed in the previous section has drawn much attention and different models have been developed and reported in the literature. In this section, a brief review of these models is presented.

1.3.1 Modeling of Time-Pressure Dispensing

Figure 1.5 shows schematically the time-pressure dispensing process. Under the assumptions that (1) the compressibility of air is ignored and (2) the fluid being dispensed is a Newtonian one, Babiarz [1999] developed a model for the time-

pressure dispensing process, in which the flow rate through the needle was expressed as a function of geometry, material viscosity, and pressure difference, i.e.,

$$Q = \frac{\pi D_n^4 (P_g - P_e)}{128 \mu L_n} \tag{1.1}$$

where Q is the flow rate, μ the material viscosity in the needle, P_g the pressure in needle hub, P_e the pressure at needle outlet, L_n the length of needle, and D_n the diameter of needle.

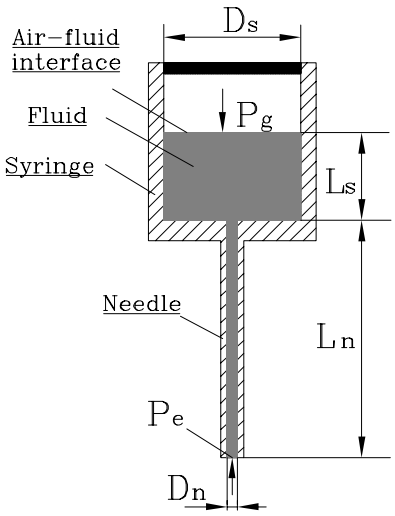

Figure 1.5 Schematic of time-pressure dispensing

Equation (1.1) shows clearly that the flow rate is dependent on the viscosity of the material in addition to the pressure difference. Please note that the simple model is valid only for dispensing Newtonian fluids. However, most fluids used in the electronics packaging usually exhibit non-Newtonian behaviour, thereby limiting the application of this model. Considering the non-Newtonian fluid behaviour, there

are also some studies carried out to improve the model. For example, Razban [1993] developed a model based on Power-law equation. However, in his model, the flow rate represented is of steady state. In other words, this model is not valid for capturing the dynamics of the flow rate. Chen [2002] took into account the influence of the air compressibility and fluid non-Newtonian behaviour and developed a model representative of the dynamics of the flow rate. On this basis, the investigation into the dynamics and its influence on the small fluid amount dispensed was carried out. As the model was developed based on the general power-law equation for the fluid flow behaviour, it is not valid for other non-Newtonian fluids such as viscoelastic fluids. Considering the air compressibility, Zhao *et al*. [2006] also developed a model for the dynamics of the flow rate in the time-pressure dispensing process. During the model development, Zhao *et al*. also used the power-law equation, which limits the applications to other non power-law fluids.

1.3.2 Modeling of Rotary Screw Dispensing

The flow rate in the rotary screw system shown in Figure 1.6 has a more complex dependency on the materials viscosity, the geometry of the pump as well as the pressure difference than the time-pressure dispensing system does. In addition, it also depends on the syringe rotation speed.

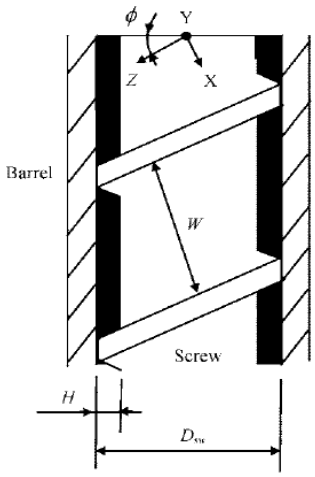

Figure 1.6 Schematic of rotary screw dispensing

Rauwendaal [1986] developed a flow rate model under the assumptions: 1) Newtonian fluid, 2) incompressible, steady state fluid, and 3) the viscosity is temperature-independent. The flow rate is then expressed by

$$Q = n_t \frac{\omega D_{sw} W H \cos\phi}{2} F_d + n_t \frac{W H^3 (P_1 - P_2) \sin\phi}{12 l_a \mu} F_p \qquad (1.2)$$

where Q is the flow rate, μ the material viscosity in auger, n_t the number of parallel threads, ω the rotational speed of the screw, ϕ the syringe lead angle, W the pitch distance, D_{sw} the inside diameter of syringe, H the distance between the thread root and syringe wall, l_a the total length of syringe, P_1 the pressure at the auger inlet, P_2 the pressure at auger outlet & needle inlet, and F_d and F_p are the geometric form factors.

The first term on the right side stands for the drag flow rate caused by screw rotation; the second term is the pressure-driven flow rate, which is proportional to

the pressure gradient in the channel. The model is still being used in many real applications [Babiarz 1999]. Same as the time-pressure model (1.1), model (1.2) is not applyied to non-Newtonian fluids. Furthermore, it cannot predict the dynamics of the flow rate. Realizing the weakness, Rauwendaal [2004] reported a new model based on model (1.2) for non-Newtonian power law fluids.

$$Q = \frac{(4+n)\omega D_{sw} WH\cos\phi}{20} + \frac{WH^3(P_1 - P_2)}{4K(1+2n)l_a}\left(\frac{D_{sw}\omega\cos\phi}{2H}\right)^{1-n} \tag{1.3}$$

where k is the power law consistency index with a unit of $Pa \cdot s^n$ and n the power law index.

Although the model is used for non-Newtonian fluid, it just represents the flow rate in the screw channel, rather than the dynamics of flow rate occurring in the dispensing process.

Chen [2007] and Hashemi [2006] noticed these two points and made the following improvements based on equation (1.3):

- Developed the models for the entire process, which included the flow rates in the syringe and in the needle.
- Developed a dynamic model, which describes the relationship between the flow rate and screw rotation speed. The model is convenient for controlling a small fluid amount dispensed within a short time.

1.3.3 Modeling of Positive Displacement Dispensing

Babiarz [1999] developed a simple model for the positive displacement dispensing system, which is simply a function of the piston speed and piston diameter. The model is given by

$$Q = V_p \pi D_p^2 / 4 \tag{1.4}$$

where Q is the flow rate, V_p the piston motion velocity, and D_p the diameter of piston.

From the model, it can be seen that the flow rate is proportional to the piston moving speed and piston diameter. The linear relationship implies that the fluid behaviors such as viscosity and compressibility do not affect the flow rate. While this may be true for dispensing a large amount of fluid, it is not true for dispensing small amount of fluid. When dispensing small amount of fluid, the dispensing process becomes complicated due to the fluid compressibility and behaviors [Chen *et al*. 2003]. As most fluids dispensed exhibit non-Newtonian flow behaviour, the fluid flow in the syringe under the action of a piston is generally transient, non-Newtonian, compressible and viscous. It is noted that such a flow is complex due to the coupling between non-Newtonian flow behaviour and compressibility. To the author's knowledge, this has not been well addressed in the literature to date.

1.3.4 Brief Review of Liquid Bridge Breakage and its Mechanism

Liquid bridges are the bodies of fluid anchored between two solid supports and held by capillary forces as shown in Figure 1.7.

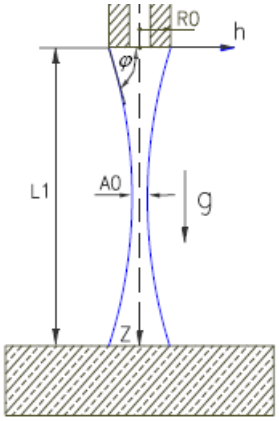

Figure 1.7 Diagram of a Liquid Bridge

In terms of the properties of the fluid, liquid bridges can be classified into two categories: Newtonian and non-Newtonian. In liquid bridges research, the instability and breakage mechanism are the focus of both academic and practical interest. For a weightless right circular cylinder Newtonian liquid bridge, the well-known Rayleigh stability limit holds [Espino *et al.,* 2002]: "The liquid column becomes unstable when its length is larger than its undisturbed circumference". Many studies were carried out on liquid bridges which are different from the ideal configuration. For example, Meseguer [1983] analyzed the influence of axial micro-gravity on the breakage of axisymmetric slender liquid bridges. He also studied the stability of slender, axisymmetric liquid bridgers between unequal disks [Meseguer, 1984; Meseguer *et al.,* 2003]. Slobozhanin and Perales [1993] investigated the stability of axisymmetric liquid bridges between equal disks in an

axial gravity field. Meseguer *et al.* [1999] analyzed influences of many perturbations on the ideal configuration, such as nonaxial acceleration. As for the research on the breaking of Newtonian liquid bridge, an historical review of the representative publications can be found in Zhang *et al.*[1996], Eggers [1997], and Yildirim and Basaran [2001]. None of those studies address the issue of extensional viscosity in the breakage process.

For non-Newtonian liquid bridge breakage, in the study of polymer melts rupture at high rates of extension, Vinogradov and his co-workers [Joshi and Denn 2003] constructed a master curve of extension strain at rupture as a function of extension rate as seen in Figure 1.8. They proposed four regimes of failure at increasing elongation rates as described below, each regime has different extension strain-rate features.

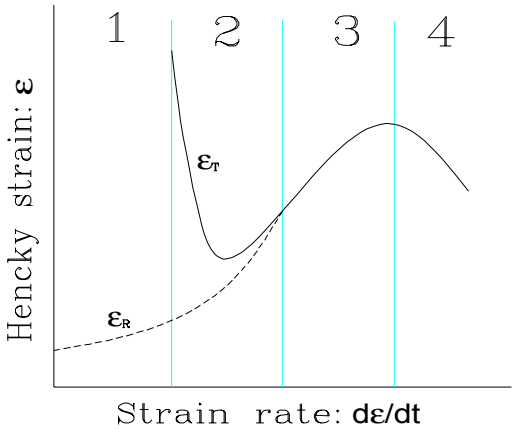

Figure 1.8 Master curve of uniaxial extension of polymer liquids
[Joshi and Denn 2003]

(1) Flow regime - occurs at a very low extension rate. Here, the response of the liquid bridge is dominated by viscous flow. Surface tension effects are often

important in this regime, and the failure is caused by a surface tension-driven instability through a ductile failure ("necking"). The recoverable (elastic) strain increases with the extension rate, but it is very small relative to the total strain at failure.

(2) Transition regime- superposition of elastic deformation and viscous extensional flow take place in this regime. However, steady flow appears impossible because the liquid bridge breaks before a steady flow regime can be realized.

(3) Rubbery regime- there is virtually no flow in this regime and the entire deformation is completely elastic and there is nearly complete recovery of the strain following rupture. The total strain at rupture increases with the extension rate in this regime.

(4) Glassy zone- occurs at very high rates of strain. The rupture is a brittle failure, the tensile stress and strain at the rupture both decrease with the extension rate, and the strain is completely recoverable.

Figure 1.9 shows the ruptures schematically, which happens in flow regime, transition regime, rubbery regime, and glassy regime respectively from left to right.

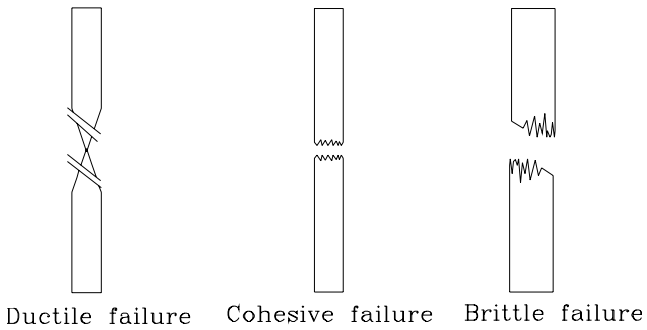

Figure 1.9 Non-Newtonian liquid bridge failures

Based on their research on deformation of viscous filaments, McKinley and Sridhar [2002] also summarized the two most common types of breakage, i.e., capillary breakage, and elastic thread breakage. The capillary breakage happens at low extension strain regions. When the viscous bridge is undergoing elongation, owing to the large capillary pressure in the neck, the liquid bridge necks decrease rapidly. Once the local necking rate is larger than the extensional scale, the motion near the midplane will undergo a finite time singularity. An interesting phenomena observed by Spiegeberg and McKinley [1996] was that the response of non-Newtonian fluid is initially very similar to Newtonian fluid under strain less than two, but under high level strain, a non-Newtonian fluid shows different behaviour than Newtonian fluid. As for elastic thread breakage, it is thought to be caused by the "strain-hardening" phenomenon [Spiegelberg *et al.,* 1996]. Once the extension strain is bigger than one value, the faster increase in the transient extension viscosity of the central region will render this section less susceptible to further deformation. With the further extension, the sections adjacent to the central region will continue to deform until they also strain-harden to the same level experienced by the central part of the bridge. Finally, the extensional strain and tensile stress along the bridge is becoming more and more uniform, the liquid bridge radius becomes progressively more axially uniform at large strains and hence leads to an increasingly homogeneous extensional deformation. Once the "strain hardening" process uniforms the deformation, the bridge extends as a purely elastic extension, which is corresponding to the rubbery regime in the Master curve. When the breakage happens, it is an elastic thread break-up, or the cohesive failure in Figure

1.9. The failure mechanism for the slender fluid column is dramatically different from the capillary-driven breakage observed in Newtonian fluid, which exhibits no strain-hardening behaviour [Yao *et al.,*1998]. In the above studies, it's worthy to note that the extensional viscosity and the extension strain have been addressed to explain the breakage process.

It should be noted that although the breakage mechanism mentioned above help to better understand the liquid bridge breaking process, they are only general physical descriptions of breaking process based on extension experiments. Apparently, a quantitative tool is still needed to resolve the real engineering problems such as in fluid dispensing applications to calculate fluid amount dropping onto the board

1.4 The Existing Issues of Positive Dispensing and Research Objectives

Figure 1.10 shows a typical positive displacement dispensing process. Briefly, it includes two steps. First, the dispensing apparatus is transported to the dispensing point and a desired volume of fluid is extruded through the needle. When the dispensed fluid amount is very small or the dispensing duration time is short, due to the influences of fluid compressibility and behaviour, the volume dispensed out of the needle is not equal to the displacement of the moving piston. This is the first problem that needs to be addressed. Second, once the fluid is dispensed, due to the action of the fluid surface tension, it flows onto the target surface and forms a liquid bridge between the needle and the target surface. When the dispensing head is lifted

straight up to the retracted position, the liquid bridge is deformed and will be broken. The second process is dominated by the fluid extensional deformation. After breaking, part of the fluid transfers onto the board and the rest stays on the needle rim. It is obvious therefore the volume that drops onto the board is not equal to the fluid volume extruded out of the needle. This is considered one common problem with the positive-displacement method as well as the other two methods. Currently, various designs of fluid dispensing systems exist. However, no studies have been done to evaluate and compare these different designs on a common basis. How to evaluate the three dispensing methods and optimize the selection of dispensing methods is a problem of industrial importance. To address these issues, three objectives are set in the present study.

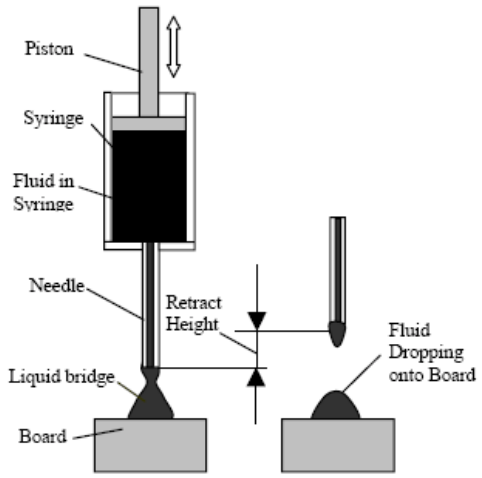

Figure 1.10 Typical positive-dispensing process diagram

1. Develop a dynamic model for the positive displacement dispensing method.

As a promising dispensing method being extensively used in electronics assembly, the positive-displacement dispensing method has not been investigated

for the purpose of developing a dynamic model like what had been done for the time-pressure and rotary screw dispensing methods. Simple models, such as one given in Equation (1.3), cannot meet current precise dispensing requirements; and a more accurate dynamic model is desirable. The model should consider the non-Newtonian fluid behaviour, fluid compressibility, dispensing duration time, and fluid level in the syringe.

2. Develop a model to represent the fluid transferred onto the subplate.

As the fluid amount transferred onto the board is not equal to the fluid dispensed out of the needle, how to calculate the fluid on-board is a critical problem when a small amount of fluid is dispensed. To solve the problem, a liquid bridge breakage model is necessary to predict the fluid amount transferred onto the board. Developing such a model to express the non-Newtonian liquid bridge deformation and breakage and calculate the fluid amount on a board is the second objective of the present work.

3. Evaluation of fluid dispensing systems using axiomatic design principles.

An evaluation is presented in this study by means of axiomatic design principles. The results from such an evaluation will not only allow users to choose the appropriate systems for given applications, but also facilitate designers to develop new dispensing systems.

1.5 Organization of the Thesis

This thesis consists of six chapters, including this chapter. Other chapters are briefly described as follows.

Chapter 2 discusses the non-Newtonian fluids classification and their characteristics. Different models are reviewed and their applications are discussed. A specific 3-parameter power-law model is derived for the FP4451 fluid that is used in the present work.

Chapter 3 deals with the development of a dynamic model of the positive-displacement method. The fluid compressibility in the syringe and general power-law fluid are taken into account in the modeling. Based on the dynamic model, simulations are carried out to investigate the influence of needle temperature, fluid level in syringe, dispensing time, fluid compressibility as well as fluid behaviour on flow rate.

Based on existing theories of liquid bridge and Laplace's equation, a model to represent the fluid amount transferred to the board is proposed in **Chapter 4**. This model is then used in simulations to investigate the influence of both the surface tension and the initial fluid amount dispensed out of needle outlet on the fluid amount transferred to the board.

Chapter 5 presents an evaluation of the dispensing systems designs by means of the Independence Axiom and the Information Axiom. Also, included in this chapter is the development of an algorithm for computing the information content of redundant designs.

The conclusions drawn from this research are given in **Chapter 6**, along with suggestions and recommendations for possible future work.

2. FLOW BEHAVIOUR OF ENCAPSULANT MATERIALS

2.1 Encapsulant Materials for Electronics Packaging

In electronics packaging, encapsulants are used to protect semiconductor devices and interconnects (e.g. wire bonding and solder bumps) from moisture, ozone, ultraviolet radiation, and damage caused by thermal shock and low & high temperature cycling, as well as to increase their long-term reliability [Wong, 1998].

Common encapsulant materials include urethane, epoxy or silicone polymers [Yang *et al.*, 2003]. Urethane encapsulants offer good solvent resistance, have good low temperature properties, but tend to degrade at high temperatures. Thus, urethane is usually used in applications where thermal expansion is not a concern. Epoxies are one of the most widely used polymers in electronics packaging. The key chemical and physical properties attractive to packaging applications include excellent chemical and corrosion resistance, electrical and physical properties, excellent adhesion, thermal insulation, low shrinkage, and reasonable material cost [Wong, 1998]. However, the temperature stability of epoxies is a concern [Yang, 2003]. In contrast, silicone is based on a stable silicone backbone and able to offer excellent adhesion to a variety of surfaces. Silicones have been used in a variety of cases where there is a high temperature duty or a high extreme in thermal cycling [Yang, 2003].

2.2 Fluid Flow Behaviour

The flow behaviour of a fluid is used to describe the relationship of the shear stress and shear rate in the fluid. Based on the behaviour exhibited, fluids can be classified into two categories: Newtonian and non-Newtonian. Newtonian fluids are those exhibiting a linear relationship between shear stress and shear rate [Skelland, 1967]. Thus

$$\tau = \mu \frac{du}{dy} \tag{2.1}$$

where u is velocity of the fluid, y is a position coordinate, du/dy is velocity gradient called the shear rate, μ is viscosity, and τ is shear stress.

Fluids that do not show the linear relationship between shear stress and shear rate are non-Newtonian fluids [Steffe, 1996]. Examples of non-Newtonian fluids include polymer melts, blood, and materials possessing both viscous and elastic properties. Non-Newtonian fluids can be further divided into three groups [Skelland, 1967]

- Time-independent non-Newtonian fluids

For these kinds of non-Newtonian fluids, the shear rate and shear stress relationship can be expressed as:

$$f(\tau) = \frac{du}{dy} \tag{2.2}$$

where f is a non-linear function. Figure 2.1 shows several types of the fluids.

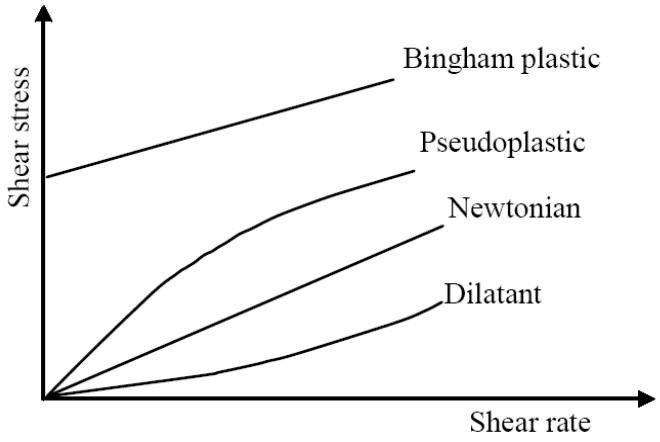

Figure 2.1 Time-independent non-Newtonian fluids

In this figure, dilatant liquids display increasing viscosity with increasing shear. The shear viscosity of pseudoplastic liquids decreases with an increase of shear rate and has a shear thinning behaviour.

- Viscous time-dependent non-Newtonian fluids

Time-dependent fluids are those for which the shear rate is a function of both magnitude and duration of shear. The relationship between shear rate and shear stress can be expressed as [Wan, 2005]:

$$f(\tau, t) = \frac{du}{dy} \tag{2.3}$$

where t is the time.

Time-dependent fluids are usually classified into two groups: thixotropic fluids and rheopectic fluids, depending on whether the shear stresses decrease or increase

with time at a given shear rate and constant temperature. For thixotropic fluids, the materials exhibit a reversible decrease in shear stress with time at a given shear rate and constant temperature. If a shear stress- rate curve is measured in a single experiment in which shear rate is steadily increased from zero to a maximum value and then immediately decreased steadily toward zero, a form of hysteresis loop would be obtained, as shown in Figure 2.2.

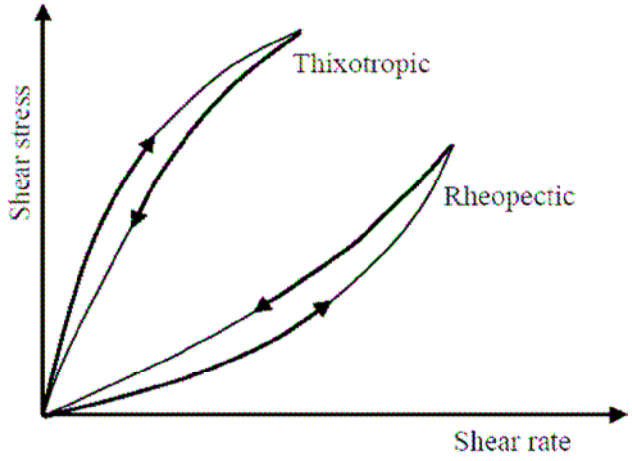

Figure 2.2 Time-dependent non-Newtonian fluids

The arrows in Figure 2.2 indicate the chronological progress of the experiment.

Rheopectic fluids are the materials exhibiting a reversible increase in shear stress with time at a constant shear rate under isothermal conditions. The location of the hysteresis loop for a given fluid is again dependent on the time history of the material, including the rate at which *du*/*dy* is increased and decreased during the experiment.

- Viscoelastic non-Newtonian fluids

Viscoelastic non-Newtonian fluids are materials which combine the elastic properties of solids with the flow behaviours of fluids. In a purely Hookean elastic solid, the stress

corresponding to a given strain is independent of time, whereas for viscoelastic substances the stress will gradually dissipate. In contrast to time-independent non-Newtonian fluid, viscoelastic fluids flow when subjected to stress, but part of their deformation is gradually recovered upon removal of the stress [Skelland, 1967].

2.3 Models for the Time-Independent Fluid Flow Behaviour

A general equation to describe the flow behaviour of time-independent, non-Newtonian fluids is the Herschel-Bulkley (H-K) model [Steffe, 1996]

$$\tau = k(\dot{\gamma})^n + \tau_0 \tag{2.4}$$

where τ is the shear stress, k the consistency coefficient, n the flow behaviour index, $\dot{\gamma}$ the shear rate, and τ_0 the yield stress.

Equation (2.4) is of shear stress-shear rate form. In engineering applications, the apparent viscosity, which is defined as the ratio of the shear stress to the shear rate, is always used in modeling fluid behaviour. So, in apparent-viscosity form, Equation (2.4) can be rewritten as

$$\eta = f(\dot{\gamma}) = k(\dot{\gamma})^{n-1} + \frac{\tau_0}{\dot{\gamma}} \tag{2.5}$$

where η is the apparent viscosity.

Equation (2.5) can also be used to represent the flow behaviour of Newtonian, power-law, and Bingham plastic fluids depending on the values of n and τ_0. Specifically, for Bingham fluids, n =1, thus Equation (2.5) is reduced to

$$\eta = k + \frac{\tau_0}{\dot{\gamma}} \tag{2.6}$$

An important characteristic of the Bingham fluids is the presence of a yield stress τ_0 which represents a finite stress required to achieve flow.

For general power-law fluids, the model is shown in Equation (2.7). There are two different types power-law fluids, depending on value of n. One is shear shinning (pseuodoplastic) if $0 < n < 1$ and the other one is shear thickening (dilatant) if $1 < n < \infty$.

$$\eta = k(\dot{\gamma})^{n-1} \tag{2.7}$$

Figure 2.3 shows the apparent viscosity versus shear rate of time-independent fluids. It is seen that, for $n > 1$, the plot of η versus $\dot{\gamma}$ goes upward and the material is dilatant or shear-thickening, and that, for $n < 1$, the plot of η versus $\dot{\gamma}$ goes downward and the behaviour is shear-thinning.

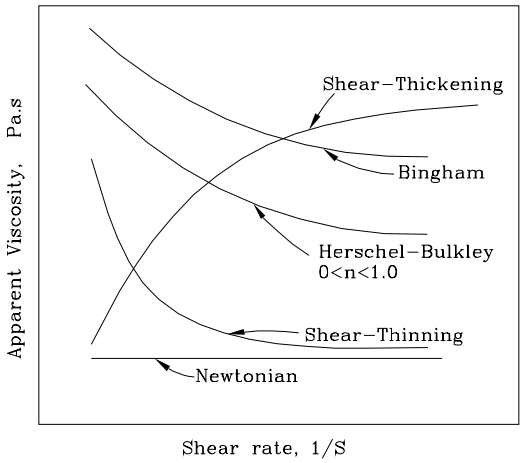

Figure 2.3 Apparent viscosities of time-independent fluids [Steffe, 1996]

The shear-thinning power-law model of Equation (2.7) fits the experimental results for many materials at the middle shear rate over two or three decades on logarithmic scales. Taking a polymer melt as an example, the range is 10^2-10^4 s^{-1} [Barnes *el at.*, 1989]. The power-law model is used extensively to describe non-Newtonian fluid properties in theoretical analysis as well as in calculations applied to the engineering applications such as polymer manufacturing processes. However, the model can't represent the shear stress when shear rate is small and high.

Shear thinning behaviour is very common in polymer melts [Steffe, 1996]. During the flow, shear thinning materials exhibit three distinct regions, as shown in Figure 2.4, in which the slope of the curve represents the apparent viscosity. In the lower region, η_0 (called the zero shear viscosity) is approximately a constant with changing shear rates; in the middle region, the apparent viscosity η changes dramatically with shear rate; and in the upper region, η_∞ (called the limiting

viscosity at infinite shear rate) is approximately a constant regardless of the change in the shear rate. [Barnes el at., 1989]

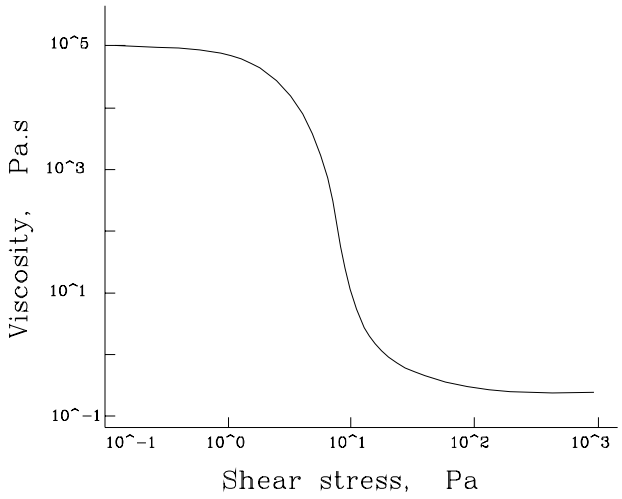

Figure 2.4 Apparent viscosity versus shear rate of shear thinning behaviour

For the complete shear rate range, the shear thinning power-law model, i.e., (2.7), fails to represent the fluid behaviour in the lower and upper regions [Barnes *et al.*, 1989]. Cross proposed the following improved model [Steffe, 1996]

$$\frac{\eta_s - \eta_\infty}{\eta_0 - \eta_\infty} = \frac{1}{1 + (c\dot{\gamma})^n} \tag{2.8}$$

where η_0 and η_∞ refer to the asymptotic values of viscosity at very low (zero-viscosity) and very high shear rates respectively, and c is a constant with the dimension of time.

A comparison between the shear-thinning power-law model (2.7) and the Cross model (2.8) is given in Figure 2.5. It illustrates that the shear thinning power-law works only in the central region.

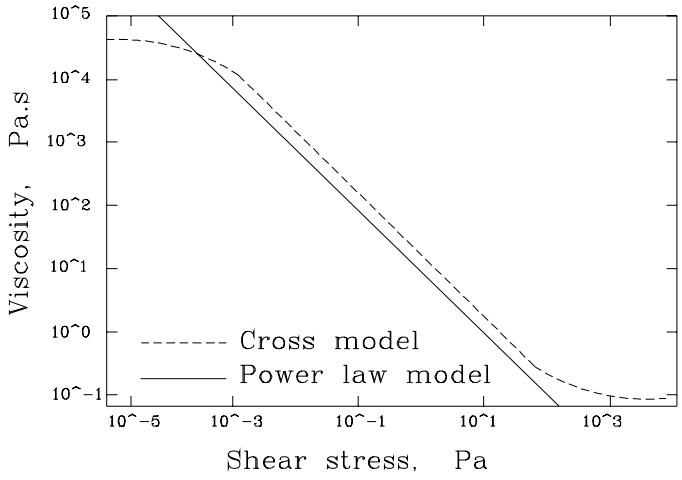

Figure 2.5 Comparison of power law model to Cross model

In the lower region, as $\eta_0 >> \eta_\infty$, a so called 3-parameter Carreau model is developed to cover the lower and center shear rate region [Barnes *et al.,* 1989]:

$$\eta = \eta_0 \left(1 + (c_1 \dot{\gamma})^2\right)^{\frac{n-1}{2}} \tag{2.9}$$

where c_1 has the similar significance to the c of the Cross model (2.8).

2.4 3-Parameter Carreau Model for Fluid Hysol FP4451

In this section, the 3-Parameter Carreau Model for the Hysol FP4451 fluid (supplied by Dexter Corporation) is presented based on the previous experiments conducted in the author's lab. The Hysol FP4451 fluid is a kind of non-Newtonian

fluid and is used in die encapsulation in electronics packaging. The derived model is used in the following chapters.

Chen and Ke [Chen and Ke, 2006] investigated the flow behaviour of the Hysol FP4451 fluid at different temperatures by using a Brookfield rheometer. The measured results of the shear viscosity versus the shear rate at various temperatures are given in Figure 2.6. This figure suggests that FP4451 is a shear –thinning non-Newtonian fluid. By fitting the results, Chen and Ke [2006] determined n to be 0.5672.

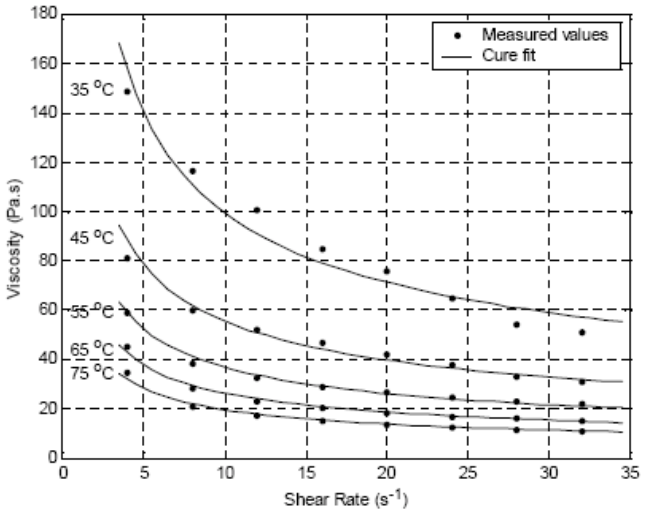

Figure 2.6 Viscosity versus shear rate at various temperatures

A specific 3-Parameter Carreau Model for Hysol FP4451 fluid at 45°C can be developed with the method described here: by picking up different experimental data under different shear rate provided by the 45°C curve in Figure 2.7 and submitting these data into the Equation (2.7), the k is calculated having the best

value of 156.532 to match the curve. Therefore, the 45°C curve of shear viscosity versus shear rate is expressed by general power law model as:

$$\eta = 156.532\dot{\gamma}^{0.5672-1} \tag{2.10}$$

The equation is verified to identify the curve by the comparison (see Table 2.1) of data calculated by Equation (2.10) and measurement data from Figure 2.6.

Table 2.1 Viscosity data comparison between Equation (2.10) and 45°C curve

Shear rate 1/S	Viscosity by Equation (2.10), Pa.s	Viscosity from 45°C curve, Pa.s
5	77.999	80
10	57.783	58
15	48.483	48
20	42.807	42
25	38.866	38
30	35.917	36
35	33.599	33

Since the shear thinning power-law model (2.10) covers only central shear rate range, it cannot include the lower shear rates which will be used in the present work. Therefore, a specific 3-parameter Carreau model (2.9) is needed based on (2.10). Based on shear rate and viscosity values shown in Table 2.1calculated by model (2.10), submitting these data into Equation (2.9) to set up a group of equations, the constant parameters η_0 and k_1 can be figured out. After calculation, the 3-parameter Carreau model is expressed as below

$$\eta_s = 728.5\left(1+\left(34.9\dot{\gamma}\right)^2\right)^{\frac{0.5672-1}{2}} \tag{2.11}$$

Figure 2.7 clearly compares the 3-parameter Carreau model (2.11) and power-law model (2.10). From the two curves, when shear rate is bigger than 0.1/s, the 3-parameter Carreau model has almost the same curve as the power-law model. However, when the shear rate is less than 0.1/s, the two models have different shapes and the difference is getting bigger when shear rate is becoming smaller.

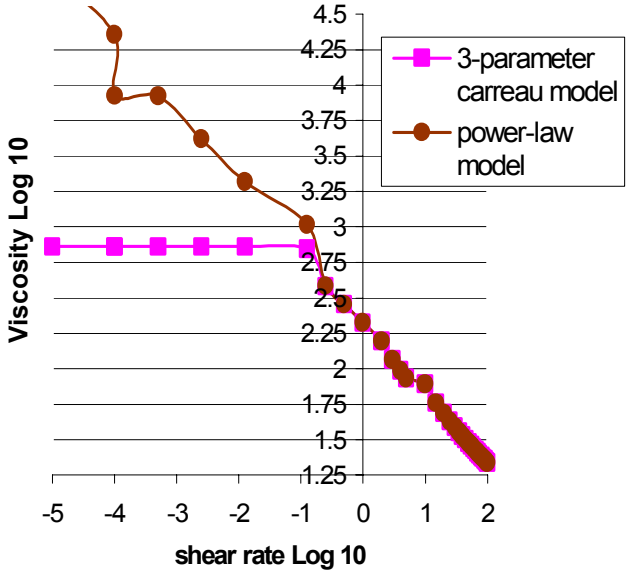

Figure 2.7 Power-low (2.10) curve versus 3-parameter Carreau curve (2.11)

2.5 Summary

This chapter presents a brief introduction to the flow behaviour of the encapsulant materials used in electronics packaging. It is noted that the flow behaviour exhibited by most fluids used in electronics packaging is time independent and one of the distinct characteristics of the flow behaviour is a non-

linear relationship between shear stress and shear rate at a given temperature. Various equations for modeling the time-independent and non-linear relationship are reviewed and examined in this chapter. Also, based on the previous experiments on the fluid Hysol FP4451, a 3-parameter Carreau model for the fluid is derived for use in the present study.

3. MODELING OF THE VOLUME OF FLUID OUT OF NEEDLE

3.1 Introduction

Positive-displacement dispensing is recognized as the most promising approach since it is assumed to be 'true' volumetric dispensing [Soron, 1997], i.e., the flow rate or the volume of fluid dispensed is dependent only on the piston movement but not on the properties of the fluid being dispensed. This can usually be considered true for dispensing a large volume of fluid with continuous piston motion. As the dispensed volume of fluid decreases to the microliter range, however, this assumption is no longer valid because both fluid compressibility and fluid flow behaviour can significantly affect the flow rate. As a result, under identical operational conditions, the volume of fluid dispensed varies with such factors as fluid level left in the syringe, fluid temperature, and dispensing duration time. Therefore, ensuring consistency in the volume of fluid dispensed is difficult and demanding. This is considered one of the major problems occurring in the positive-displacement dispensing process. To resolve this problem, a model to represent the flow rate or the volume of fluid dispensed is obviously desirable. This chapter presents the development of such a model by taking into account the influence of both fluid compressibility and fluid flow behaviour. Based on this model, simulations are carried out to investigate the dispensing process performance, with emphasis on identifying the influence of the fluid volume left in the syringe, the needle temperature, and the fluid properties on the consistency in fluid volume dispensed.

3.2 Modeling of Positive-Displacement Dispensing Processes

In the positive-displacement dispensing process, the fluid flow in the syringe and the needle are important. Therefore, it is logical to develop a model for the positive-displacement dispensing process by means of two major steps: (1) representing the pressure in the syringe and 2) representing the flow rate in the needle under this pressure.

3.2.1 Pressure in the Syringe

Given that most fluids dispensed exhibit non-Newtonian flow behaviour, the fluid flow in the syringe under the action of piston is generally transient, non-Newtonian, compressible, and viscous. Such a flow is quite complex due to the coupling between non-Newtonian flow behaviour and compressibility. To the author's knowledge, this has not been well addressed in the literature to date. To simplify this problem, the following assumptions are made for the fluid flow in the syringe:

(1) Only fluid compressibility is considered by neglecting the influence of non-Newtonian flow behaviour and the minor losses. This is reasonable if the fluid velocities in the syringe are small. Furthermore, the pressure in the syringe is assumed uniform due to the fact that the height of fluid level in syringe is short so that the time required for pressure waves to propagate through the fluid is small in comparison with the time scale of interest.

(2) The syringe is isothermal as the temperature in the dispensing process is usually well-controlled, which eliminates the need for an energy equation in the model.

Under these assumptions, the lumped parameter approach employing the continuity equation can be used to represent the pressure in the syringe, P, which is given by [Merritt, 1967]

$$A_p \dot{X} - Q = \frac{V_0 - A_p X}{B} \frac{dP}{dt} \tag{3.1}$$

where Q is the flow rate out of the syringe or the flow rate entering the needle, X the piston position in the syringe, A_p the cross-section area of the piston, V_0 the initial fluid volume in the syringe, and B the bulk modulus of the fluids.

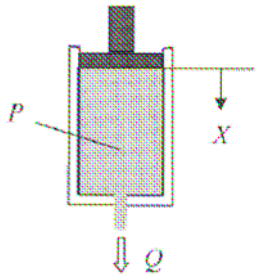

Figure 3.1 Piston descending and driving fluid out of syringe

3.2.2 Flow Rate of Fluid Dispensed

Under the pressure in the syringe, the fluid in the needle is driven out and dispensed, as illustrated in Figure 3.2.

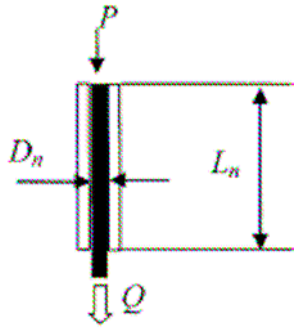

Figure 3.2 Pressure-driven flow in the needle

For such a pressure-driven flow, the flow rate can be significantly influenced by the flow behaviour of the fluid being dispensed. It is known that, if a fluid exhibits non-Newtonian flow behaviour, the relationship between the shear stress and the shear rate in the fluid is non-linear. The H-K power law model is the most widely used and is given by

$$\tau = \tau_0 + k\dot{\gamma}^n \tag{3.2}$$

Physically, τ_0 is the critical value of shear stress at which fluid yields or starts to flow, k is a measure of viscousness - the higher k, the more viscous the fluid, and n is a measurement of the degree of rheological behaviour - the greater departure of n from unity, the more pronounced the rheological behaviour. For a given fluid, the values of n, τ_0, and k are determined experimentally. In particular, n is usually identified as a constant and τ_0 and k as functions of temperature [Chen, 2002; Han and Wang, 1997].

For the fluid flow in the needle, it is assumed

- the fluid in the needle is incompressible considering that the fluid volume in the needle is small in comparison with that in the syringe, which implies the flow rate entering the needle is the same as that out of the needle, i.e., the flow rate of fluid dispensed,
- the fluid properties are time-independent and the flow is laminar, and
- there is no slip between the fluid and the needle wall.

Under these assumptions, the flow rate of fluid dispensed can be derived and its transfer function is given by [Chen *et al.*, 2002]

$$\frac{Q(s)}{P(s)} = \frac{Q_u}{\rho L_n \frac{Q_u}{A_n} s + 1} \tag{3.3}$$

where ρ is the fluid density, L_n the length of the needle, A_n (or $\pi D_n^2/4$) the cross-section area of the needle, and Q_u the steady-state flow rate under a unit pressure, depending on the fluid flow behaviour and the needle geometry.

For the fluid characterized by the generalized power law (Equation 3.2), Q_u is given by [Nakayama *et al.*, 1980]

$$Q_u = \frac{\pi D_n^3}{8Pk^{1/n}\tau_w^3}(\tau_w - \tau_0)^{(n+1)/n} \left[\frac{n}{3n+1}\tau_w^2 + \frac{2n^2}{(2n+1)(3n+1)}\tau_w\tau_0 + \frac{2n^3}{(n+1)(2n+1)(3n+1)}\tau_0^2\right] \tag{3.4}$$

where τ_w is the shear stress at the needle wall under the applied pressure.

Taking into account the minor losses due to the effect of the needle entrance and exit, τ_w is [Chen *et al.*, 2000]

$$\tau_w = \frac{D_n}{4L_n}\left(P + L_n \rho g - 1.12\,\rho u^2\right) \tag{3.5}$$

where g is the gravity acceleration, and u the average velocity of the fluid in the needle which is given by Q/A_n.

It should be noted in the above equation that the pressure drop due to the surface tension at the fluid meniscus formed at the needle exit is ignored. If the needle diameter is small enough, however, this pressure drop should be considered and should appear in above Equation (3.5).

Combining Equation (3.3) with the Laplace transform of Equation (3.1) yields a transfer function for the flow rate of fluid dispensed to the velocity of the piston motion, which is given by

$$\frac{Q(s)}{\dot{X}(s)} = \frac{A_p}{a_2 s^2 + a_1 s + 1} \tag{3.6}$$

where

$$a_1 = \frac{V_0 - AX}{BQ_u} \quad \text{and} \quad a_2 = \frac{\rho L_n (V_0 - AX)}{BA_n} \tag{3.7}$$

From the above equations, it can be seen that the dynamics of the flow rate of fluid dispensed is equivalent to a second order system. Its steady-state value is a function of the piston cross-section area, A_p. This is commonly recognized in industry

nowadays. The transient of the flow rate is dependent on the position of piston (X) in addition to the fluid compressibility (B) and the fluid flow behaviour (through Q_u). It is noted that X is not constant over a dispensing process and increases as the process proceeds. As a result, the dynamics of the flow rate varies with the piston position or the fluid volume left in syringe. So do the volumes of fluid dispensed by the identical operational conditions. This is illustrated in details in the following section.

3.3 Investigation of the Positive-Displacement Dispensing Process Performance

In this section, an investigation into the performance of the positive-displacement dispensing process is carried out based on the model presented in the previous section. The objective is to identify the influence of the duration of piston motion, the fluid volume in the syringe, the needle temperature, the fluid flow behaviour, and the fluid compressibility on the consistency in fluid volume dispensed.

The system parameters used in this study are listed in Table 3.1, while the fluid properties are given in Table 3.2.

Table 3.1 Original system parameters for simulation

Parameter	Value
Piston motion velocity, $\dot{x}$	0.04 mm/s
Dispensing time, t_d	0.2 s
Piston or syringe diameter, D_p	25 mm
Syringe capacity, C	60 cc
Length of needle, L_n	16 mm
Internal diameter of needle, D_n	1.0 mm
Needle temperature, T	45^o C
Fluid level in syringe*	50%

* The fluid level in syringe = (fluid volume in syringe/ syringe capacity) x 100%

Table 3.2 Fluid properties

Parameter	Value
Density, ρ	1780 kg/m^3
Bulk modulus, B	1.0x10^9 Pa
Flow behaviour index, n	0.6
Yield stress, τ_0	$9.22 \times e^{80.98/T}$ Pa
Consistency index, K	$25.39 \times e^{92.47/T}$ Pa $\cdot$ s^n

In particular, the parameters of n, τ_0, and k in Table 3.2 for the characterization of fluid flow behaviour using Equation (3.2) are taken from a previous study [Chen, 2002] in which n was identified as a constant and τ_0 & K were, based on the measured data of τ-$\dot{\gamma}$, correlated to temperature (i.e., T with unit of ^{O}C) by using exponential functions with the values of curve-fitting parameters given in Table 3.2. These operational conditions and fluid properties are used in all simulations presented in this chapter except where specified. To measure the consistency in fluid volume dispensed, the relative error was used and is given by

$$Error = \frac{\int_0^t Q dt - A_p \dot{X} t_d}{A_p \dot{X} t_d} \times 100 \ \% \tag{3.8}$$

where the term of $A_p \dot{X} t_d$ is the volume displaced by the piston motion, in which t_d is the dispensing time or the duration of the piston motion; t is the integration time (6 s in this study) and the term of $\int_0^t Q dt$ is the volume of fluid dispensed, in which the flow rate, Q, is simulated in Matlab based on the model developed. The block diagram of this simulation is shown in Figure 3.3.

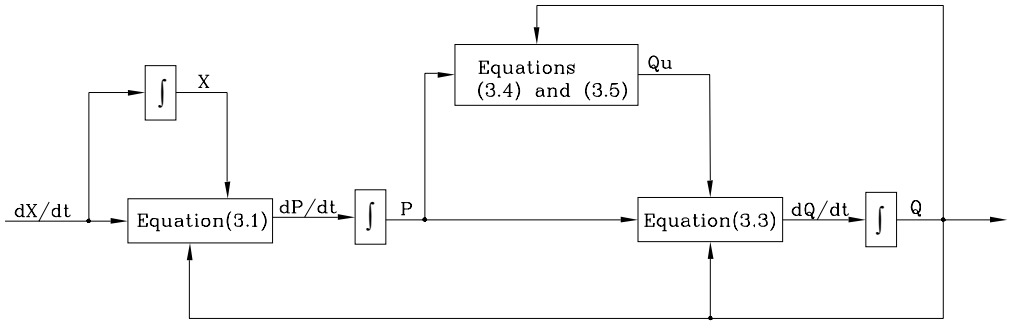

Figure 3.3 Block diagram for simulating the flow rate of fluid dispensed

3.3.1 The Influence of Dispensing Time

Using different values of the dispensing time, t_d, the pressure in syringe, P, and the flow rate, Q, were simulated and the results are shown in Figure 3.4 for t_d = 0.08, 0.2, 1.0, and 3.0 s.

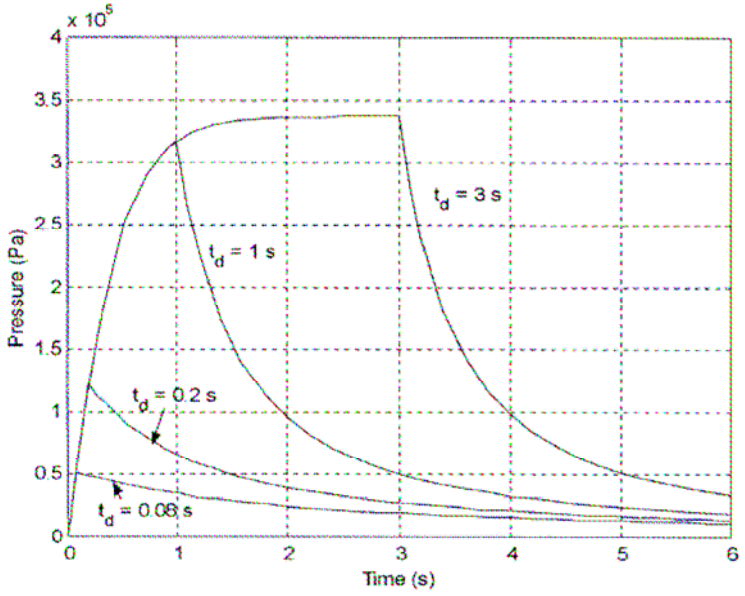

(a) Pressures in the syringes

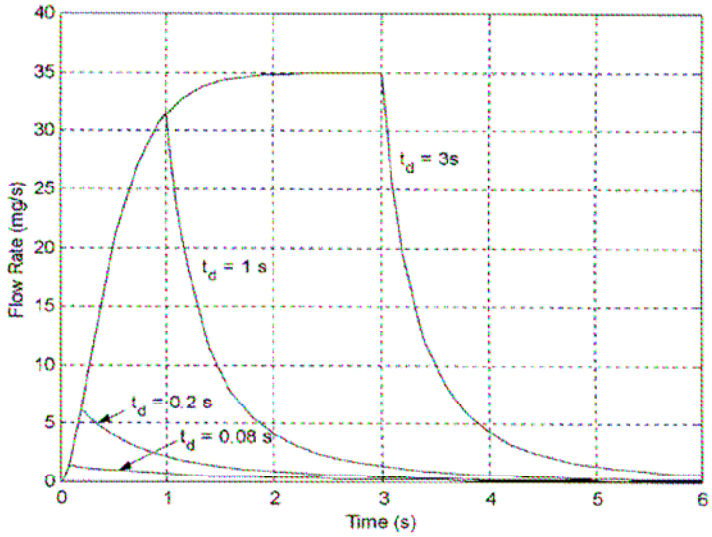

(b) Flow rates of fluid dispensed

Figure 3.4 Influence of dispensing time

The results indicate that, for small t_d, P and Q do not reach their steady-state values.

In such cases, the dynamics of the flow rate is critical to the fluid volume dispensed.

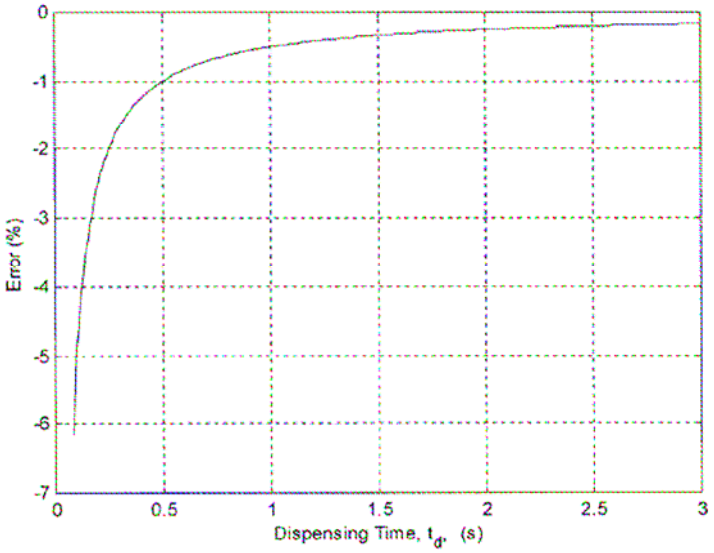

Figure 3.5 Relative error versus t_d

Figure 3.5 shows the calculated relative errors at different values of t_d using Equation (3.8). It can be seen that, as t_d increases, the error decreases and approaches zero, implying that the influence of the flow rate dynamics can be ignored. However, if t_d is less than 0.5 s in this simulation, the error starts to increase significantly. This indicates that the positive-displacement approach is no longer a true volumetric dispensing technique.

3.3.2 The Influence of Fluid Level in Syringe

At different levels of fluid in the syringe, the flow rates were simulated and the results are shown in Figure 3.6 for t_d = 0.2 s.

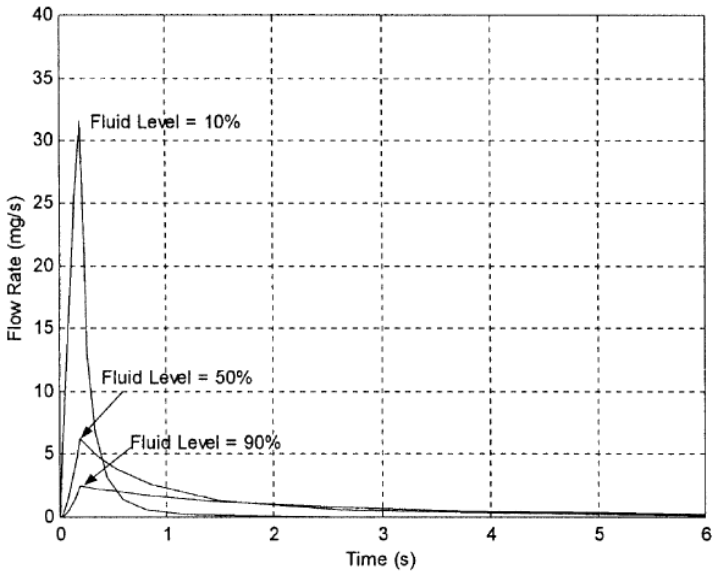

Figure 3.6 Flow rates at different fluid levels in syringe for t_d = 0.2 s

This illustrates that the fluid level in the syringe can dramatically affect the dynamics of the flow rate, thereby changing the fluid volume dispensed. To measure the influence of fluid level on the fluid volume dispensed, the relative

errors were calculated over a dispensing process, i.e., the fluid level changing from full to empty; and the results are shown in Figure 3.7 for t_d = 0.08, 0.2, and 1.0 s.

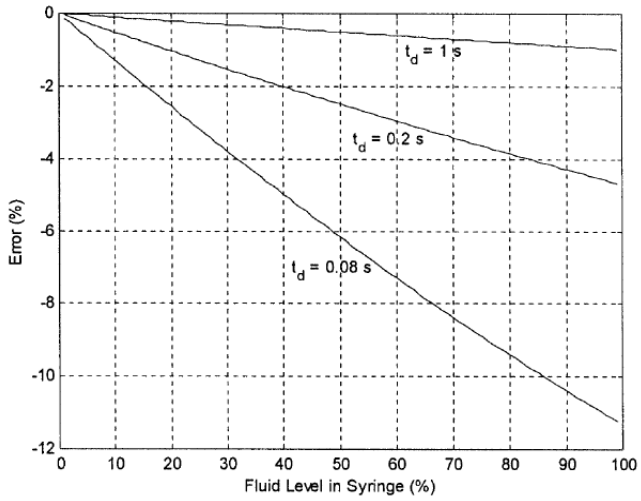

Figure 3.7 Relative error versus the fluid level in syringe

It can be seen that the relative errors over a dispensing process are not constant but dependent on the fluid level in the syringe. Furthermore, the inconsistency becomes worse with the decrease in t_d or the decrease in the fluid volume required to be dispensed.

3.3.3 The Influence of Needle Temperature

It is known that the fluid behaviour is dependent on the needle temperature as the fluid flows through the needle. As a result, the needle temperature can also affect the flow rate and the volume of fluid dispensed. In this simulation, the dependence of fluid behaviour on the needle temperature given in Table 3.2 was used. For temperatures of 35°C, 45°C, and 55°C, the simulated flow rates and the calculated relative errors are shown in Figure 3.8 and Figure 3.9.

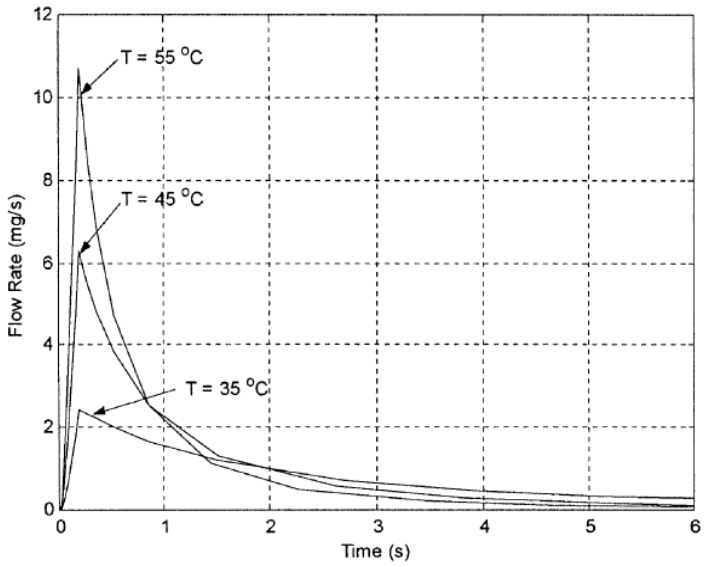

Figure 3.8 Influence of needle temperature: flow rate

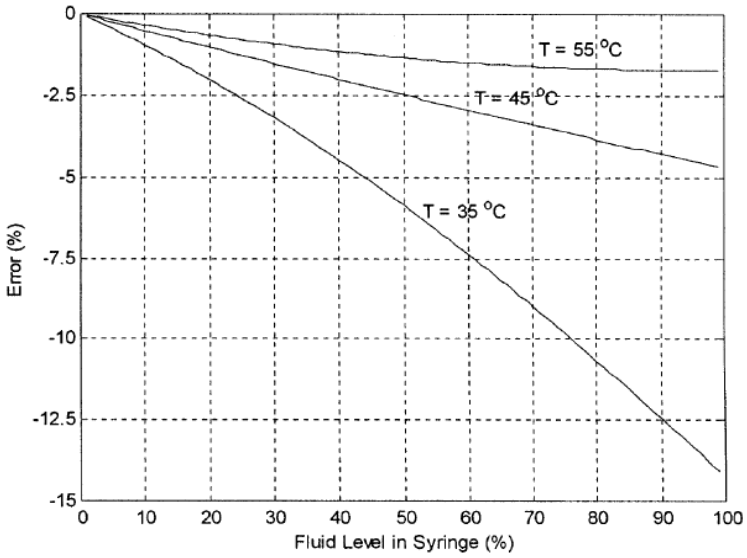

Figure 3.9 Influence of needle temperature: relative error versus the fluid level

It is seen that the temperature can significantly change the dynamics of the flow rate and thereby the consistency in fluid volume dispensed. Particularly, the lower the temperature, the slower the transient response of the flow rate and the more pronounced the inconsistency in fluid volume dispensed.

3.3.4 The Influence of Fluid Flow Behaviour

If a fluid exhibits time-dependent flow behaviour, the shear rate in the fluid depends on not only the shear stress magnitude, but also the shear stress duration and the time lapse between consecutive applications of shear stress (or shear history) [Skelland, 1967]. As a result, the flow behaviour varies with respect to time, depending on the shear history that the fluid experiences. In addition, it is also known that the flow behaviour of fluids for electronics/MEMS packaging might be quite different from batch to batch. All of the resulting differences in fluid flow behaviour can be represented by appropriately modifying the parameters of τ_0, n, and k given in Equation (3.2) [Chen *et al.*, 2003]. In this simulation, as an example, different values of n are chosen to illustrate its influence on the consistency in fluid volume dispensed. Figure 3.10 and 3.11 shows the simulated flow rates and the calculated relative errors for n = 0.4, 0.6, and 0.9.

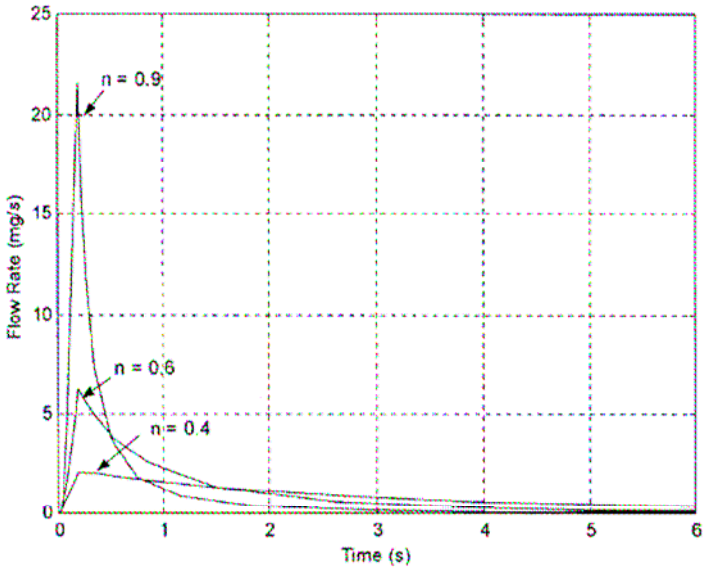

Figure 3.10 Influence of fluid flow behaviour: flow rate

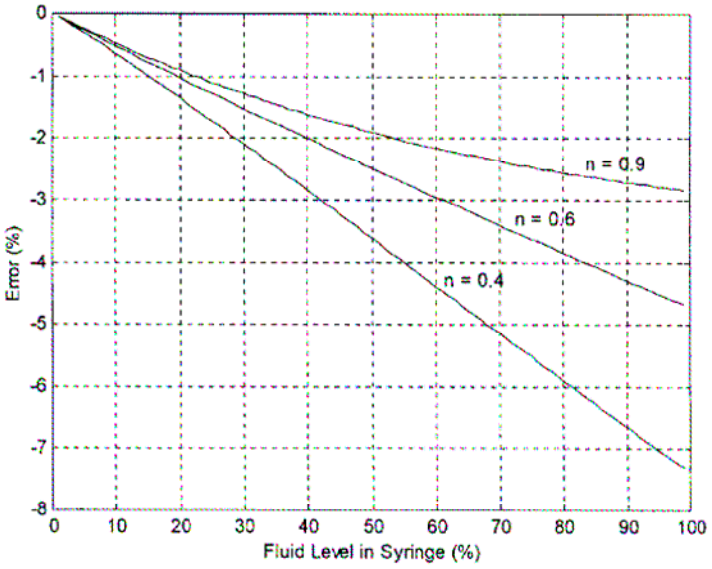

Figure 3.11 Influence of fluid flow behaviour: relative error versus fluid level in syringe

It is seen that the greater departure of n from unity, the slower the transient response of flow rate and the more pronounced the inconsistency in fluid volume dispensed.

3.3.5 The Influence of Fluid Compressibility

Fluid is compressible, which is represented by the bulk modulus, B, in this study. To illustrate the influence of fluid compressibility, different values of B were chosen for simulating the flow rates and calculating the relative errors. The results are shown in Figure 3.12 and 3.13 for $B = 0.5\times10^9$, 1.0×10^9, and 4.0×10^9 Pa.

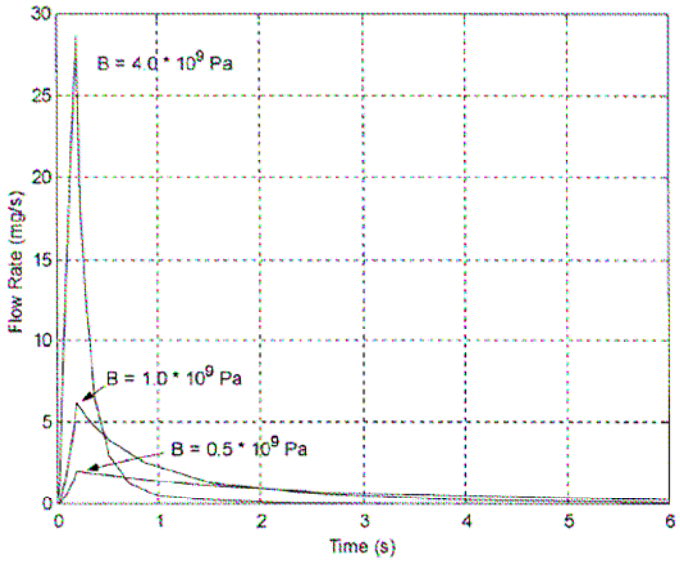

Figure 3.12 Influence of fluid compressibility: flow rate

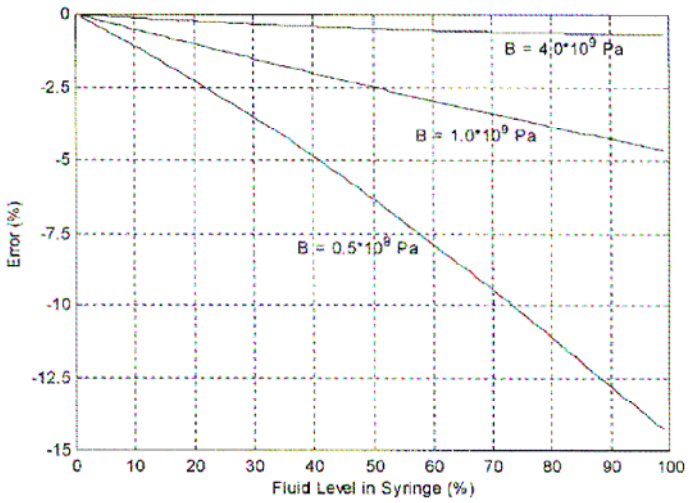

Figure 3.13 Influence of fluid compressibility: relative error versus fluid level in syringe

It is seen that the fluid compressibility can significantly change the dynamics of the flow rate and thereby the consistency in the fluid volume dispensed. In particular, the more pronounced the fluid compressibility, the slower the transient response of flow rate and the more pronounced the inconsistency in fluid volume dispensed.

3.4 Summary

Positive-displacement dispensing is the most promising among several approaches used in industry. Its performance, however, is also affected by the fluid properties if it is used to dispense minute volumes of fluid. This chapter presents the development of a model for the positive-displacement dispensing process, which accounts for these effects. Based on this model, an investigation into the process performance was carried out with the following conclusions:

(1) The dynamics of the flow rate of fluid dispensed is equivalent to a second order system. Its steady-state value is a function of only the piston cross-section area, as commonly recognized in industry; and the fluid level in syringe, the needle temperature, and the fluid properties affects its transient. In particular, the higher fluid level in syringe, the lower needle temperature, or the more pronounced non-Newtonian behaviour and compressibility of the fluid can result in the slower transient response of flow rate.

(2) Due to the dynamics of flow rate, the volume of fluid dispensed is different from the volume displaced by the piston motion. This difference becomes more pronounced with a decrease in the dispensing time or a decrease in the fluid volume needed to be dispensed. This indicates that the positive-displacement approach is not a true volumetric dispensing process.

(3) The flow rates of fluid dispensed are inconsistent over a dispensing process, depending on the needle temperature and the fluid properties. The lower needle temperature or the more pronounced non-Newtonian behaviour or

compressibility of the fluid, the more pronounced inconsistency in fluid volume dispensed can be resulted. This suggests that, for improving the consistency over a dispensing process, the needle be heated to improve fluid flow in the needle. Meanwhile, syringes of smaller size should be used to reduce the change in fluid level in the syringe over a dispensing process.

4. MODELING OF FLUID AMOUNT TRANSFERRED ONTO A BOARD

4.1 Introduction

Understanding the dispensing process is the first step in modeling fluid dispensed onto a board. Figure 4.1 shows the typical operations in the dispensing process. The dispensing head carries the needle moving down to the contact position (Figure 4.1 (a)) so that the fluid contacts the board surface and, by surface tension, the fluid rapidly flows to the board and forms a liquid bridge between the needle and the board (Figure 4.1 (b)). Then, the needle is moved upward vertically (Figure 4.1 (c)) and the bridge deforms into a necked configuration until the bridge is broken into two parts: one part flows onto the board and the other part still hangs on the needle (Figure 4.1 (d)).

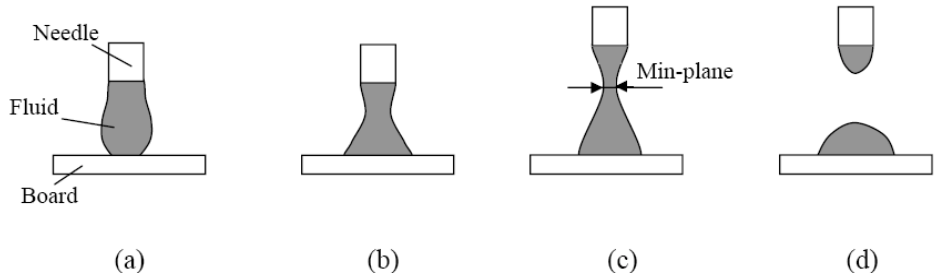

Figure 4.1Typical processes of dispensing fluid from the needle to the board

The above process indicates that the fluid amount extruded out of the needle is different from the fluid amount finally transferred to the board. The difference is considered one major problem affecting dispensing performance, especially in the case where the dispensed fluid amount is minute. This problem exists in all three dispensing methods: positive-displacement, air-pressure, and rotary-screw

dispensing. To solve the problem, it is necessary to develop a model to represent the fluid amount transferred to the board.

This chapter presents the development of such a model and a simulation study based on the developed model. In particular, in Section 4.2 two relevant concepts of extensional viscosity and liquid breakage criteria are introduced; in Section 4.3 a model is developed to determine the bridge breakage and then to determine the fluid amount transferred to the board; and in Section 4.4 a simulation study is presented based on the developed model, which is followed in Section 4.5 by the summary and conclusions.

4.2 Extensional Viscosity and Breaking Criteria

4.2.1 Extensional Viscosity

As reviewed and discussed in Chapter 1, a great deal of theoretical and experimental work has been done to look into the stability and breakage issues of liquid bridges. For Newtonian liquid bridges, the research focuses on the axisymmetric equilibrium and stabilities under various disks configurations, aspect ratios, and gravity levels. In the area of non-Newtonian liquid bridge, however, efforts are concentrated on the bridge extensional deformation process, the constitutive equation of extensional viscosity, and the bridge breaking mechanism. As most materials dispensed in the electronic packaging process are non-Newtonian fluids, the extensional viscosity in non-Newtonian liquid bridges is introduced in this section.

Figure 4.2 shows schematically the geometry for an ideal liquid bridge in a filament-stretching device. It is called an ideal bridge if the liquid bridge shape is always symmetrical and uniform during the extension, the radii of the top and the bottom plates are equal, and the weight of the liquid is ignored.

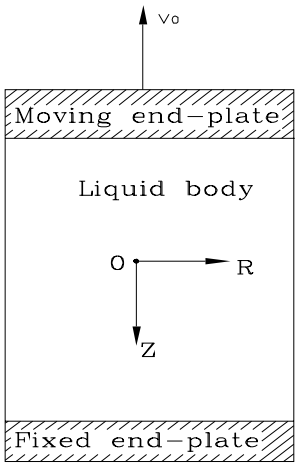

Figure 4.2 Geometry of the liquid bridge in filament stretching devices [Yao *et al.,* 1998]

In a uniaxial extension, the fluid body is extended in one direction with respect to the size reduction in the other two directions. To measure the uniaxial extensional deformation, the Hencky strain, which is defined by evaluating an integral from initial length L_0 to the extended length L, is used

$$\varepsilon_h = \int_{L_0}^{L} \frac{dl}{L_0} = \ln(L/L_0) \tag{4.1}$$

where ε_h is the Hencky strain.

In an Eulerian steady extension flow, if extension velocity v_0 is constant, the relationship between the v_0 and extension rate $\dot{\varepsilon}$ in the Z direction can be described by

$$v_0 = \dot{\varepsilon} L(t) \tag{4.2}$$

where L(t) is the instantaneous liquid bridge length during the extension.

From Equation (4.2), extension rate is derived as

$$\dot{\varepsilon} = \frac{v_0}{L(t)} = \frac{v_0}{L_0 + v_0 \cdot t} \tag{4.3}$$

According to the mass conservation law, for such an ideal extension, the radius of the liquid bridge varies from the initial value R_0 in the following form,

$$r(t) = R_0 \sqrt{\frac{L_0}{L(t)}} \tag{4.4}$$

where R_0 is the initial radius of the liquid bridge and $r(t)$ the liquid radius at time t.

Thus, the ideal real-time cross-section area of the bridge $A(t)$ can be derived and given as

$$A(t) = \pi r^2(t) = \pi R_0^2 \times \frac{L_0}{L_0 + v_0 \cdot t} = A_0 \frac{L_0}{L_0 + v_0 \cdot t} \tag{4.5}$$

Practically, however, Yao *et al*. [2000] found that for an extension shown in Figure 4.2 with a constant extension rate $\dot{\varepsilon}$, the local strain rate at the axial mid-plane $Z = L(t)/2$ was 50% higher than the imposed $\dot{\varepsilon}$. As a result, the relationship

between the extended length $L(t)$ and the mid-plane radius $R_{mid}(t)$ is expressed as [McKinley and Sridhar, 2002]:

$$\frac{L(t)}{L_0} = \left(\frac{R_0}{R_{mid}(t)} \right)^{4/3} \tag{4.6}$$

To explain the phenomena, it is noted that the real uniaxial extension is not a pure extension deformation due to the existence of shearing effects close to the two end-plate regions because of the pinning of fluid elements adjacent to the end-plates [Gaudet and McKinley, 1998].

As suggested by Equation (4.3), if extension velocity v_0 is constant and extension occurs within a very short period of time, then the extension rate is approximately a constant and the mid-plane radius is also governed by Equation (4.6). Consequently, for a bridge extension with constant velocity V_0, the real-time cross-section area at the mid-plane $L(t)/2$ is then modified from Equation (4.5) to

$$A\ (t, L(t)/2) = \pi r^2(t, L(t)/2) = \pi R_0^2 \times (\frac{L_0}{L_0 + v_0 \cdot t})^{3/2} = A_0 (\frac{L_0}{L_0 + v_0 \cdot t})^{3/2} \tag{4.7}$$

For an extension deformation, Gaudet and McKinley [1998] defined the transient extensional viscosity growth function as

$$\eta_E^+(t, \dot{\varepsilon}) = \frac{\tau_{zz} - \tau_{rr}}{\dot{\varepsilon}} \tag{4.8}$$

where τ_{zz} is the extension stress in the Z direction, and τ_{rr} the stress in the radial R direction.

According to Yao *et al.* [2000], the extension stress τ_{zz} developed at $L(t)/2$ in the Z direction is

$$\tau_{zz} = \frac{F_0}{A(t, L(t))} - \frac{\rho g L(t)}{2} - \frac{2\sigma}{r} \tag{4.9}$$

where F_0 is the force imposed on the top plate, ρ the density of fluid being stretched, σ the surface tension of the fluid, and r the cross-section radius at $L(t)/2$ position.

Meanwhile, the stress τ_{rr} in the radial direction at $L(t)/2$, due to the presence of surface tension, equals:

$$\tau_{rr} = \frac{-\sigma}{r} \tag{4.10}$$

In the mid-plane $L(t)/2$ section, submitting Equations (4.9) and (4.10) into Equation (4.8) yields the extensional viscosity, which is given by

$$\eta_E^+(t, \dot{\varepsilon}) = \frac{\left(\dfrac{F_0}{A\left(t, L(t)/2\right)} - \dfrac{\rho g L(t)}{2} - \dfrac{\sigma}{r} \right)}{\dot{\varepsilon}} \tag{4.11}$$

4.2.2 Trouton Ratio and Breaking Criteria

To calculate the total stress $\left(\frac{F_0}{A(t,L(t)/2)}-\frac{\rho g L(t)}{2}-\frac{\sigma}{r}\right)$ in Equation (4.11), it is essential to know the extensional viscosity constitutive equation $\eta_E^+(t,\dot{\varepsilon})$. Normally, there are two methods to find the extensional viscosity constitutive equation for a given fluid material:

- Conducting extensional experiments to investigate the material's extensional deformation behaviour and then developing extensional viscosity constitutive equation based on experimental results.
- Finding the relationship between the shear viscosity and extensional viscosity. The rationale behind this method is that the shear viscosity and extensional viscosity are related to each other if extension strain is small. In the present work, the extensional viscosity constitutive equation can be derived from the shear viscosity constitutive equation which is presented in Chapter 2.

For Newtonian fluids, Trouton established a mathematical relationship between extensional viscosity and shearing viscosity given as below, which is valid for all extension rates [Steffe, 1996]

$$\eta_E = 3\eta_s \tag{4.12}$$

where η_E is the extensional viscosity and η_s the shear viscosity.

Accordingly, the "Trouton ratio" was introduced as follows:

$$T_R = \frac{\eta_E(\dot{\varepsilon})}{\eta_s(\dot{\gamma})} \tag{4.13}$$

where $\dot{\gamma}$ is the shear rate.

For non-Newtonian fluids, the following limiting relation between extensional and shear viscosities is true [Ealters, 1975; Petrie, 1979]

$$\eta_E(\dot{\varepsilon})\,|_{\dot{\varepsilon}\to 0} = 3\eta_s(\dot{\gamma})\,|_{\dot{\gamma}\to 0} \tag{4.14}$$

Since extension and shear viscosities are functions of different strain rates, to remove this ambiguity, Jones *et al*., had the following definition, based on their analysis of an inelastic non-Newtonian fluid [Barnes *et al.,* 1989].

$$T_R = \frac{\eta_E(\dot{\varepsilon})}{\eta_s(\dot{\gamma})} \tag{4.15}$$

where

$$\dot{\gamma} = \sqrt{3}\dot{\varepsilon} \tag{4.16}$$

in which $\eta_s(\dot{\gamma})$ is calculated at shear rates equal to $\sqrt{3}\dot{\varepsilon}$.

Hingmann *et al.* [1994] investigated the rheological properties of non-Newtonian fluid: convertional isotactic polypropylene. It was found that for different extension rates within a short extension time, the instantaneous extension viscosity $\eta_E^+(t,\dot{\varepsilon})$ also follows the Trouton behaviour. As a result, if a liquid bridge

undergoes a short period of extension or the extension strain is small, the constitutive equation (4.15) of the extensional viscosity can be re-written as

$$\eta_E^+(t,\dot{\varepsilon}) = 3\eta_s(\sqrt{3}\dot{\varepsilon}) \tag{4.17}$$

Submitting (4.17) into (4.11) yields

$$\left(\frac{F_0}{A(t, L(t)/2)} - \frac{\rho g L(t)}{2} - \frac{\sigma}{r} \right) = \dot{\varepsilon} \cdot 3\eta_s(\sqrt{3}\dot{\varepsilon}) \tag{4.18}$$

4.3 Modeling of the Fluid Amount Transferred onto a Board

4.3.1 Breakage Criterion: the Considere Condition

As reviewed in Chapter 1, with respect to different extensional rates, there are three types of failures occurring in a liquid bridge deformation process, i.e., ductile failure, cohesive failure, and brittle failure. To predict ductile failure in a quantitative way, the Considere Criterion [Gareth *et al.,* 1999] can be used, which states that homogenous uniaxial extension of a viscoelastic filament is guaranteed provided the strain is less than the value at which a maximum occurs in the force versus extension curve. Or, conversely, the extension is unstable and a "neck" will form if the net tensile force in the filament passes through a maximum at a critical strain ε_c [Yao *et al.*, 2000]. This criterion is adopted in the present study to predict

the breakage of a non-Newtonian liquid bridge since the extension strain is assumed to be small or, in other words, the extension time is very short.

For a homogenous uniaxial extension, the area decreases by

$$A(\varepsilon) = \pi R^2(\varepsilon) = \pi R_0^2 e^{-\varepsilon} \tag{4.19}$$

where $\varepsilon = \dot{\varepsilon}_0 t$ is the extension strain and $\dot{\varepsilon}_0$ the initial extension rate.

Assuming the stress $(\tau_{zz} - \tau_{rr})$ is already known, the Considere criterion states that stability is guaranteed provided

$$\frac{dF_{ex.}}{d\varepsilon} = \frac{d}{d\varepsilon}\left[(\tau_{zz} - \tau_{rr})\pi R_0^2 e^{-\varepsilon}\right] \geq 0 \tag{4.20}$$

where F_{ex} is the total extensional force.

As a matter of fact, the mid-plane is the most easily broken section in ductile failure since the section has the minimum area along the bridge. Therefore, the breaking criterion in this study can be derived by submitting Equations (4.9) and (4.10) into Equation (4.20) and then replacing $\pi R_0^2 e^{-\varepsilon}$ by Equation (4.7), one has

$$\frac{dF_{ex}}{d\varepsilon} = \frac{d}{d\varepsilon}\left[\left(\frac{F_0}{A(t, L(t)/2)} - \frac{\rho g L(t)}{2} - \frac{\sigma}{r}\right) A_0 \left(\frac{L_0}{L_0 + v_0 t}\right)^{3/2}\right] \geq 0 \tag{4.21}$$

When the extension strain increases to ε_c and meets

$$\left.\frac{dF_{ex}}{d\varepsilon}\right|_{\varepsilon=\varepsilon_c} = \frac{d}{d\varepsilon}\left[\left(\frac{F_0}{A(t,L(t)/2)} - \frac{\rho g L(t)}{2} - \frac{\sigma}{r}\right)A_0\left(\frac{L_0}{L_0 + v_0 t}\right)^{3/2}\right]_{\varepsilon=\varepsilon_c} = 0 \qquad (4.22)$$

the liquid bridge can be treated as starting to break and ε_c is, accordingly, defined as the critical extensional strain. Submitting Equation (4.18) into Equation (4.22), one has

$$\left.\frac{dF_{ex}}{d\varepsilon}\right|_{\varepsilon=\varepsilon_c} = \frac{d}{d\varepsilon}\left[\left(\dot{\varepsilon} 3\eta_s \sqrt{3}\dot{\varepsilon}\right)A_0\left(\frac{L_0}{L_0 + v_0 t}\right)^{3/2}\right]_{\varepsilon=\varepsilon_c} = 0 \qquad (4.23)$$

Equation (4.23) can be used to determine the time when the breakage of the liquid bridge occurs for the cases where the extensional deformation strain is small.

In this study, the fluid FP4451 is used, and its shear viscosity is presented in Chapter 2 by means of the 3-parameter Carreau model, which is repeated here:

$$\eta_s = 728.5\left(1 + (34.9\dot{\gamma})^2\right)^{\frac{0.5672-1}{2}}$$

Submitting the above equation into Equation (4.17) yields the extensional viscosity equation for short extension time, i.e.,

$$\eta_E^+(t,\dot{\varepsilon}) = 3\times 728.5\left(1 + \left(34.9\times\sqrt{3}\dot{\varepsilon}\right)^2\right)^{\frac{0.5672-1}{2}} \qquad (4.24)$$

By submitting Equation (4.24) into Equation (4.18), the extension stress can be expressed as

$$\left(\frac{F_0}{A(t,L(t)/2)}-\frac{\rho\cdot g\cdot L(t)}{2}-\frac{\sigma}{r}\right)=\dot{\varepsilon}\times\eta_E^+(t,\dot{\varepsilon})=\dot{\varepsilon}\times 3\times 728.5\left(1+\left(34.9\times\sqrt{3}\dot{\varepsilon}\right)^2\right)^{\frac{0.5672-1}{2}} \tag{4.25}$$

Eventually, by submitting Equation (4.25) into Equation (4.23), the criterion for the FP4451 bridge breaking is obtained, which is given by

$$\left.\frac{dF_{ex}}{d\varepsilon}\right|_{\varepsilon=\varepsilon_c}=\frac{d}{d\varepsilon}\left[\left(\dot{\varepsilon}\times 3\times 728.5\left(34.9\times\sqrt{3}\dot{\varepsilon}\right)^2\right)^{\frac{0.5672-1}{2}}A_0\left(\frac{L_0}{L_0+v_0t}\right)^{3/2}\right]\Bigg|_{\varepsilon=\varepsilon_c}=0 \tag{4.26}$$

4.3.2 Liquid Bridge Shape

The breaking criteria Equation (4.26) is inadequate to calculate the fluid amount transferred onto board; a study of the liquid bridge shape is required to determine the volume deposited. In the steady state, the liquid bridge is governed by Laplace's equation. In this section, this equation is introduced; and then the boundary conditions of the liquid bridge concerned are established for determining the shape of the liquid bridge.

Consider an arbitrary small smooth surface as shown in Figure 4.3, in which an arbitrary point P_0 is treated as the origin of an pair of orthogonal lines AB and CD. The curvature radii of both lines at P_0 are R_1 and R_2, respectively. A circle is then drawn along the surface with a constant distance P_R to P_0. According to the theorem of Euler [Weatherburn, 1947], one has:

$$\frac{1}{r_1}+\frac{1}{r_2}=\frac{1}{R_1}+\frac{1}{R_2} \tag{4.27}$$

where r_1 and r_2 are the principal radii of curvature.

At point A, an element δl of the boundary line is subjected to a force $\sigma\delta l$ whose projection along the normal PN is

$$\sigma\delta l \sin\varphi = \sigma\varphi\delta l = \sigma\left(\frac{p_R}{R_1}\right)\delta l \tag{4.28}$$

where φ is very small.

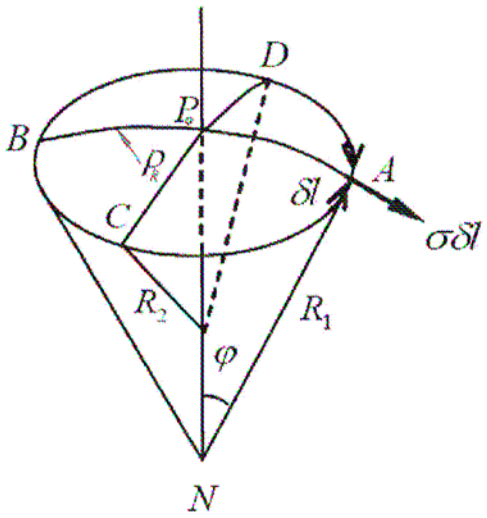

Figure 4.3 Capillary equilibrium of a non-spherical cap

Considering four elements δl of the periphery at A, B, C, and D, they will contribute the following force:

$$\sigma\delta l\left[2\left(\frac{p_R}{R_1}\right)+2\left(\frac{p_R}{R_2}\right)\right]=2p\sigma\delta l\left[\left(\frac{1}{r_1}\right)+\left(\frac{1}{r_2}\right)\right] \tag{4.29}$$

As this expression is independent of the choice of AB and CD, it can be integrated around the entire circumference. Since four orthogonal elements have been considered, the integration is made over one-quarter of a revolution, which results in

$$\pi p_R^2 \sigma \left[\left(\frac{1}{r_1} \right) + \left(\frac{1}{r_2} \right) \right] \tag{4. 30}$$

At equilibrium, this force is to be balanced by the net pressure force. Therefore,

$$\left(P'' - P' \right) \pi p_R^2 = \pi p_R^2 \sigma \left[\left(\frac{1}{r_1} \right) + \left(\frac{1}{r_2} \right) \right] \tag{4.31}$$

which reduces to Laplace's equation

$$\left(P'' - P' \right) = \sigma \left[\left(\frac{1}{r_1} \right) + \left(\frac{1}{r_2} \right) \right] \tag{4.32}$$

where P' and P'' are the pressure on the convex side and the concave side of the surface, respectively.

In the present work, Laplace's equation is used considering the gravity effect. Figure 4.4 shows schematically a liquid bridge between a dispensed needle outlet and a substrate. Here, *R0* is the outside radius of the needle, L_0 the initial distance from the needle outlet to the substrate, and *m* the mass of the fluid bridge.

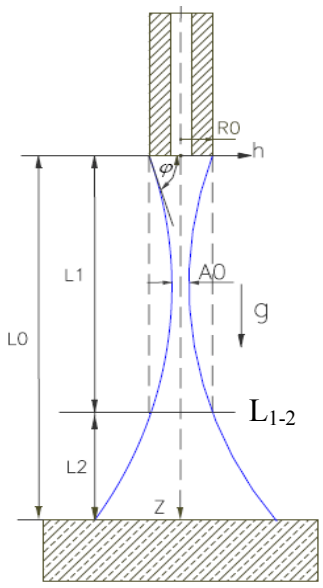

Figure 4.4 Liquid bridge between the needle and sub-plate

Taking into account the gravity effect, based on Laplace's Equation (4.32), the shape of the axisymmetric liquid bridge $h(z)$ is governed by

$$\sigma\left(\frac{1}{h(z)\left[1+(dh(z)/dz)^2\right]^{1/2}}-\frac{d^2h(z)/dz^2}{\left[1+(dh(z)/dz)^2\right]^{3/2}}\right)=P\_z(0)+\rho gz-P_0 \qquad (4.33)$$

where $P\_z(0)$ is the internal pressure in the middle point of needle outlet, P_0 the ambient pressure, z the liquid coordinate position in the z direction, $h(z)$ the liquid bridge radius in $h-z$ coordinates shown in Figure 4.4.

The boundary conditions of the liquid bridge are established as follows:

- Liquid bridge volume: $V_L=\pi\int_0^{L0}h^2(z)\,dz$ (4.34)
- Needle outlet radius: $h(z=0)=R0$ (4.35)
- Contact angle φ at $z=0$.

From Equation (4.33), it is seen that $P\_z(0)$ can affect the liquid shape. Starting from the $z=0$ section, referring to Figure 4.5, the following equations (4.36)-(4.39) link the contact angle φ to $P\_z(0)$:

$$[P\_z(0)+\rho g(\Delta z)]\pi^2 h(\Delta z)=M(\Delta z)+F_z \tag{4.36}$$

$$F_z=F_\sigma \sin\varphi \tag{4.37}$$

$$F_\sigma=2\pi h(\Delta z)\sigma \tag{4.38}$$

$$M(\Delta z)=\rho g\int_0^{\Delta z}\pi^2(R0-\Delta z\cdot tg\,\varphi)d(\Delta z) \tag{4.39}$$

where $M(\Delta z)$ is the fluid mass between the $z=0$ and $z=\Delta z$ sections, F_z the surface tension force in Z direction, F_σ the surface tension force at $z=\Delta z$ circle, and σ the surface tension.

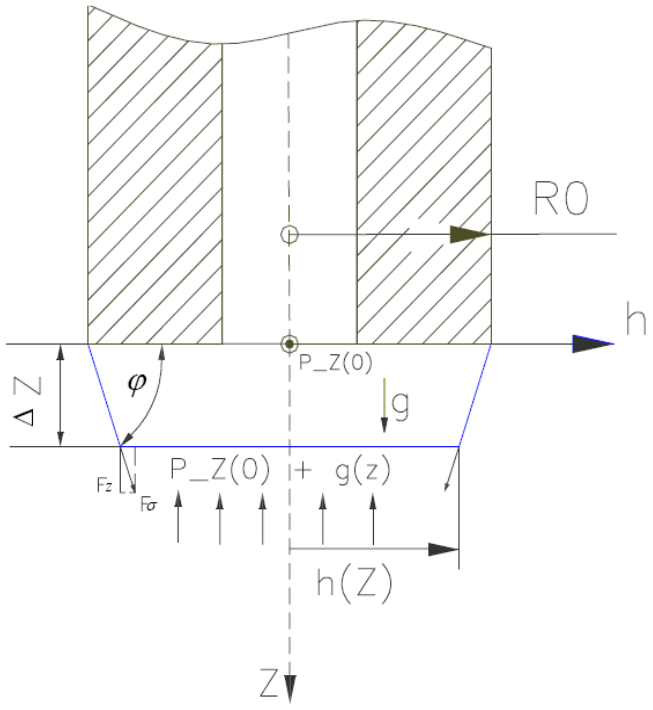

Figure 4.5 Diagram for calculating $P\_z(0)$

Submitting (4.34)-(4.36) into (4.33), when Δz is approaching zero, the solution for $P\_z(0)$ is

$$P\_z(0) = \frac{2\sigma}{R0}\sin\varphi \tag{4.40}$$

Submitting (4.40) into (4.33), the shape of the liquid bridge under gravity can be therefore expressed by

$$\sigma\left(\frac{1}{h(z)\left[1+(dh(z)/dz)^2\right]^{1/2}} - \frac{d^2h(z)/dz^2}{\left[1+(dh(z)/dz)^2\right]^{3/2}}\right) = \frac{2\sigma}{R_0}\sin\varphi + \rho g z - P_0 \tag{4.41}$$

4.3.3 Calculating Fluid Amount on a Board

It is noted that the reported studies on the liquid bridge were all carried out under the condition that top and bottom plates are of the same radius. As a result, those studies do not allow one to be able to evaluate the fluid amount on a board, which is of concern in the present study. However, the results from those studies can be adopted and used, along with the break criterion and the bridge shape model presented previously, to evaluate the fluid amount on a board. For this purpose, it is assumed that:

- There is no heat transfer between the inside and outside of the liquid bridge,
- The liquid temperatures in the syringe and needle are the same and constant. Thus, there is no impact of temperature on the surface tension. The influence of the ambient air on the surface tension is neglected as well,
- The fluid mass is small and the resultant inertial is negligible.

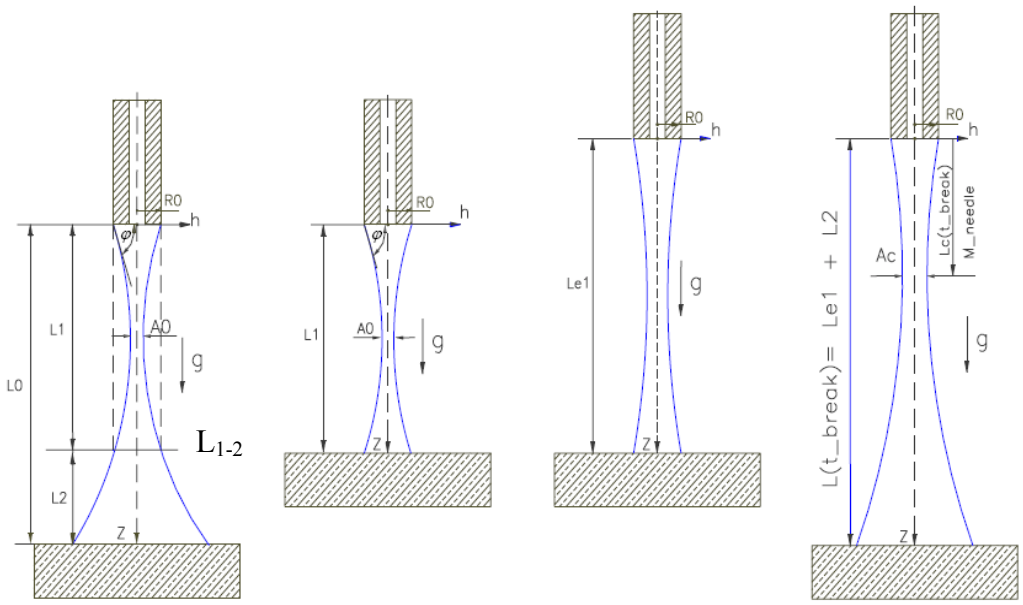

(a) (b) (c) (d)

Figure 4.6 Calculation process of fluid amount on the board

Under these assumptions, a method to evaluate the fluid amount on a board is proposed in the present study. The idea behind the method is described as followings. Once the fluid is extruded and contacts the board, the liquid bridge is considered to be in equilibrium (Figure 4.6 a); and a liquid body with identical top and bottom radii (Figure 4.6 b) can be identified within the bridge. Thus, one can apply the bridge breaking criterion presented previously to determine the breaking length as the needle moves upward (Figure 4.6 c). Finally, under the assumption that the liquid bridge with the breaking length (Figure 4.6 d) is in equilibrium, the fluid amount transferred onto the board is calculated by using the Laplace's Equation (4.41) The method consists of three steps. Details of each step are

- **Step 1**: Calculating $L1$, A0, and $M\_(L1)$ of the bridge, as shown in Figure 4.6 (a), at the initial state. Taking needle radius R0, initial bridge length L0 and

dispensed fluid amount M as boundary conditions, using Laplace's Equation (4.41) to calculate $L1$, A0, and $M\_(L1)$. Here $L1$ is the length from Z=0 to a section of the same radius $R0$, $M\_(L1)$ is the fluid mass from needle outlet to $L_{1\text{-}2}$ section, A0 is the minimum section area along the bridge. Length L2 will be used in step 3.

- **Step 2**: Obtaining the extended length $Le1$, refer to Figure 4.6 (b) and (c). In this step, $L1$ and A0 are used as initial inputs to Equation (4.26). When the extension speed V_0 is also known, from Equation (4.26), the critical extension strain ε_c will be found. Submitting ε_c into Equation (4.1), the extended length $Le1$ is acquired.
- **Step 3**: Calculating the fluid amount on the board, refer to Figure 4.6 (d). Here $Le1$ is added to L2, treating ($Le1 + L2$) as the breaking length $L(t\_break)$ before the liquid bridge is starting to separate into two parts. Taking needle radius R0 and dispensed fluid amount M as boundary conditions, re-using Laplace's Equation (4.41) to figure out the critical section which has the minimum section area Ac along the length $L(t\_break)$. The fluid amount below the critical section is then treated as the fluid amount on the board after breakage.

In the above calculation process, the length $L2$ is treated as a constant. This is reasonable given that the real extensional rate of the mid-plane section (with minimum section area) is 50 % higher than nominal extensional rate [Yao *et al.,* 2000]. This was also confirmed by the author's simulations, in which it is found that

the cross area at the $L_{1\text{-}2}$ section is much bigger than the minimum area at the section *A0*. This suggests the *A0* section and its vicinity undergoes the deformation at a faster rate than that of the $L_{1\text{-}2}$ section and the sections below. Thus, the extensional strain is mainly considered being caused by the fluid above the $L_{1\text{-}2}$ section.

4.4 Simulation Investigation and Results

Based on the model presented in the preceding section, simulations were carried out, with the objective of investigating the influence of both the surface tension and the fluid amount extruded out of a needle on the fluid amount on a board. The material used in the simulations is FP4451. The simulation procedure is the same as the aforementioned three steps when calculating the fluid amount. Based on Equation (4.41), a Simulink® model is developed to calculate parameters related to liquid bridge shape, such as $L1$, $A0$, and $M\_(L1)$, which are used for finding the critical extension strain. Given that the extension velocity v_0 is known, by using Equations (4.1) and (4.41), the critical bridge length can be found when the bridge starts to break. The fluid amount on the board can then be calculated by the Simulink® model, which is shown in Appendix I.

4.4.1 The Influence of Surface Tension

The first simulation is to investigate the impact of surface tension on the fluid amount on a board. Ten different surface tension values (Table 4.1), ranging from

0.06 N/m to 0.55 N/m, were used in the simulation, while other parameter values used are summarized in Table 4.2. In this simulation, the percentage of the fluid amount on a board to the total fluid amount dispensed is used, and the simulation results are presented in Table 4.3.

Table 4.1 Surface tension values for simulation

Case	#1	#2	#3	#4	#5	#6	#7	#8	#9	#10
Surface tension, N/m	0.06	0.08	0.1	0.155	0.2	0.25	0.3	0.35	0.43	0.55

Table 4.2 Simulation parameters for studying the influence of surface tension

Description	Value
External Diameter of the Needle, m	$R0$ = 1.06/2/1000
Initial fluid-needle contact angle at *Z=0* section	con_angle = π /3.3
FP4451 density, kg/m^3	ρ = 1780.0
Gravity acceleration, m/s^2	g = 9.8
Extension speed, m/s	v_0 = 30/1000
Total dispensed fluid amount out of needle; mg,	M = 8
Initial liquid bridge length; mm	$L0$ = 2

Table 4.3 Simulation results under different surface tension values

Case	**#1**	**#2**	**#3**	**#4**	**#5**	**#6**	**#7**	**#8**	**#9**	**#10**
Surface tension, N/m	0.06	0.08	0.10	0.15	0.20	0.25	0.30	0.35	0.43	0.55
Percentage (Fluid amount on board/Total fluid amount**)**	97.8	97.5	97.3	96.8	96.6	96.4	96.2	96.1	96.0	95.9

The simulation results are also shown in Figure 4. 7. It is seen that the fluid amount on a board can change within a small percentage of the total fluid amount extruded out of the needle due to different surface tensions. Specifically, the

percentage ratio varies from 95.9% to 97.8%, and the net change is around 2 percent of 8 mg. It is also seen that the greater the surface tension is, the less amount of fluid flows onto the board. The reason for this trend is due to the fact that the greater capillary force caused by a greater surface tension will capture more fluid around the needle outlet, thus less fluid flowing onto the board.

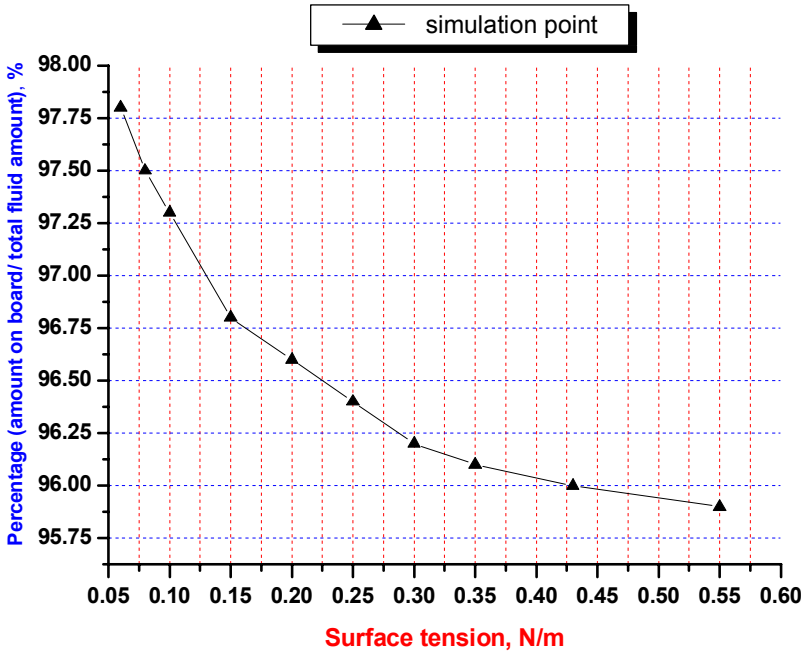

Figure 4.7 Influence of surface tension on the fluid amount on the board

4.4.2 The Influence of Initial Dispensed Fluid Amount

The second simulation is to investigate the impact of total fluid amount dispensed out of a needle on the fluid amount on the board. Eleven different surface tension values (Table 4.4), varying from 6mg to 12mg, were used. The other parameter values used are summarized in Table 4.5. As in the preceding simulation, the percentage of the fluid amount on a board to the total fluid amount dispensed is used, and the simulation results are presented in Table 4.6.

Table 4.4 Initial dispensed fluid amount for simulation

Case	#1	#2	#3	#4	#5	#6	#7	#8	#9	#10	# 11
M, mg	6	6.5	7	7.5	8	8.5	9	9.5	10	11	12

Table 4.5 Simulation parameters for studying influence of initial dispensed fluid amount

Description	Values
External Diameter of the Needle, m	*R0* = 1.06/2/1000
Initial fluid-needle contact angle at *Z=0* section	con_angle = π /3.3
Surface Tension, N/m	σ = 0.43
FP4451 density, kg/m^3	ρ = 1780.0
Gravity acceleration, m/s^2	*g* = 9.8
Extension speed, m/s	*v_0* = 30/1000
Initial liquid bridge length, mm	*L0* = 2

Table 4.6 Simulation results under different initial fluid amounts

Case	**#1**	**#2**	**#3**	**#4**	**#5**	**#6**	**#7**	**#8**	**#9**	**#10**	**#11**
***Mass*, mg**	6.0	6.5	7.0	7.5	8.0	8.5	9.0	9.5	10.0	11.0	12.0
Percentage (fluid amount on board/Total fluid amount**)**	89.2	92.1	93.0	95.1	96.0	96.7	97.3	97.8	98.1	98.6	99.0

The simulation results are also shown in Figure 4.8. It is seen that the initial dispensed fluid amount also has influences on the fluid amount on a board, i.e., the fluid amount on a board can change within a small percentage of the total fluid amount extruded out of the needle due to different fluid amount initially dispensed out of the needle. Specifically, the percentage ratio varies from 89.2% to 99.0%, and the net change is around 10 percent corresponding to the initially dispensed fluid amount from 6 mg to 12 mg. It is also seen that the greater the initial

dispensed fluid amount, the more fluid is transferred onto the board. One possible explanation for the trend is that, as surface tension is fixed, the capability of the needle to accommodate pendent fluid is also limited. With the increase of the fluid amount dispensed out of the needle, it is natural that more fluid is flowing on the board finally.

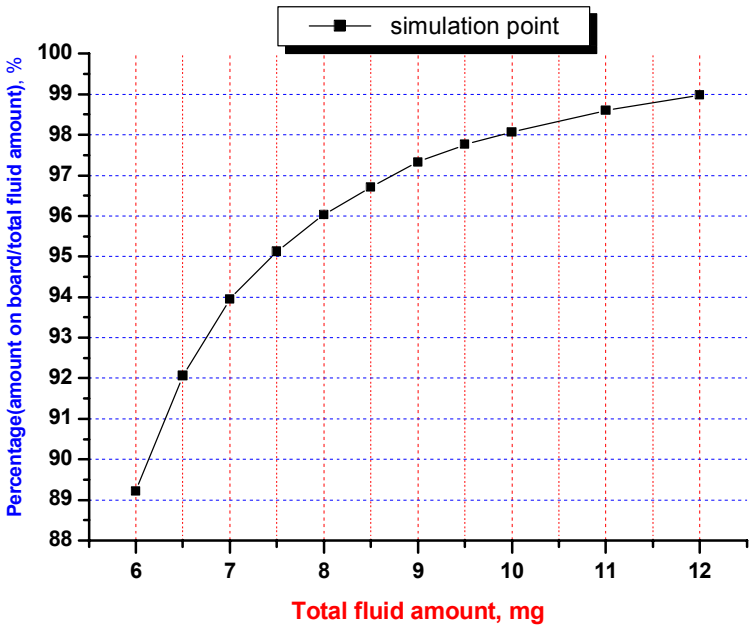

Figure 4.8 Influence of initial fluid amount on the fluid amount on the board

4.5 Summary

In the contact dispensing process, the fluid amount extruded out of the needle is different from the fluid amount finally transferred to the board. The difference is considered one major problem affecting dispensing performance. In this chapter, a model is proposed to represent the fluid amount transferred to the board based on

existing breakage theories of liquid bridge and the Laplace's equation. Based on the developed model, simulations were carried out to investigate the influences of both the surface tension and the initial fluid amount dispensed out of needle outlet on the fluid amount transferred to the board. The following conclusions have been drawn: (1) the surface tension has an impact on the extension deformation process, thereby affecting the fluid amount transferred on a board. The larger the surface tension is, the less fluid amount transferred on the board; (2) the fluid amount extruded out of the needle has a direct link to the fluid amount on the board. The more initial fluid amount is dispensed, the more fluid is transferred onto the board.

5. EVALUATION OF FLUID DISPENSING SYSTEMS

Currently, although various designs of fluid dispensing systems exist and different methods developed to model and control the dispensing systems for improved performance, there is a lack of evaluating and comparing these different designs on a common base. Obviously, this would be of great advantage for the user when choosing the dispensing system for a specific application, and for the designer when developing new dispensing systems. This chapter presents such an evaluation by means of axiomatic design principles. In particular, axiomatic design principles are briefly reviewed first in section 5.1. Second, section 5.2 introduces the redundant design and how to compute Information Content of redundant designs. At last, in section 5.3, based on the flow rate models of the three fluid dispensing systems, an evaluation of the three system designs is presented by means of axiomatic design principles.

5.1 Brief Review of Axiomatic Design Principles

Axiomatic design is one of the most powerful design approaches and has been widely used in various engineering design processes. In the axiomatic approach, design is modeled as a mapping process between functional requirements (FRs) and design parameters (DPs) and represented mathematically by [Suh, 2001],

$$\{\mathrm{FR}\} = [A]\ \{\mathrm{DP}\} \tag{5.1}$$

where $[A]$ is called the design matrix, and its element, A_{ij}, represents the sensitivity of FR_i to DP_j, i.e., $A_{ij} = \partial \mathrm{FR}_i / \partial \mathrm{DP}_j$. Usually, A_{ij} is determined based on either the

model of the product/system or the designer's knowledge on the product/system if the model is not available.

One of the principles used in axiomatic design is the Independence Axiom, which states [Suh, 2001] "the FRs must always be maintained independent of one another by choosing appropriate DPs." To satisfy the Independence Axiom, the design matrix [*A*] must be either diagonal or triangular. If it is diagonal, each of the FRs can be satisfied independently by means of one DP and such a design is termed uncoupled. If the design matrix is triangular, the independence of FRs can be guaranteed if and only if the DPs are determined in a proper sequence and such a design is termed decoupled. Any other form of the design matrix does not meet the Independence Axiom and the design resulted is said to be coupled. Therefore, if several FRs need to be satisfied, design should be carried out such that a diagonal or triangular design matrix can be resulted. For a given task defined by a set of FRs, it is likely that different designs can be resulted, all of which may be acceptable in terms of the Independent Axiom. However, one of these designs is likely to be best [Suh, 2001]. To determine the best design, the Information Axiom needs to be used, which states [Suh, 2001] "among the designs that are equally acceptable from the functional point of view, the design with the minimum information content is the best design."

The information content (I) of a given design is defined in terms of the probability (P_{FR}) of success or satisfying all of its FRs [Suh, 2001], i.e.,

$$I = \log_2 \frac{1}{P_{FR}} \tag{5.2}$$

In the case that DPs are uniformly distributed, P_{FR} can be expressed in terms of the system range, the design range, and their intersection called the common range [Suh, 2001; Frey *et al*., 2000], i.e.,

$$P_{FR} = \frac{\text{Common range}}{\text{System range}} \tag{5.3}$$

Figure 5.1, as an example, shows graphically these three ranges for a uncoupled design and a decoupled design, both of which have 2 FRs. FR_i^* denotes the targeted value of FR_i, ΔFR_i the design range of FR_i, and χFR_i the extreme value of the random variation in FR_i due to the random variation in DPs (denoted by δDP_i). In particular, for the uncoupled design χFR_i is given by

$$\chi\text{FR}_i = \left|A_{ii}\delta\text{DP}_i\right| \qquad i = \{1, 2\} \tag{5.4}$$

where $\left|A_{ii}\delta\text{DP}_i\right|$ denotes the extreme value of $A_{ii}\delta\text{DP}_i$. Note that the use of $\left|\cdot\right|$ to indicate the extreme value is also employed in the rest of this Chapter . The system range is the area of the rectangle, as shown in Figure 5.1(a), which is symmetrical about the axes of FRs. For the decoupled design, χFR_i can be affected by several DPs and given by, if its design matrix is given in the lower triangular form

$$\chi\text{FR}_i = \sum_{j=1}^{i}\left|A_{ij}\delta\text{DP}_j\right| \qquad i = \{1, 2\} \tag{5.5}$$

The system range is the area of the parallelogram, as shown in Figure 5.1 (b), which is symmetrical about the targeted values $(\text{FR}_1^*, \text{FR}_2^*)$. Once the system range is determined,

from Figure 5.1 one can readily determine the common range (i.e., the intersection of the system range and the design range), for which readers may refer to [Suh, 2001]. Eventually, the information content can be calculated by using Equations (5.2) and (5.3).

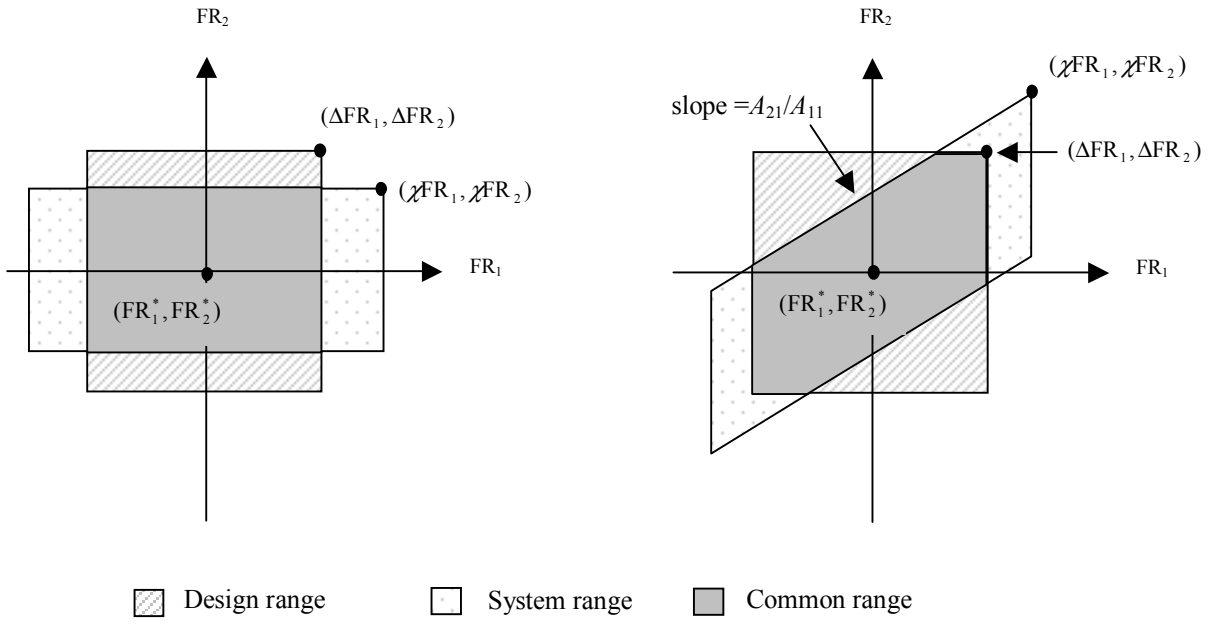

(a) uncoupled design (b) decoupled design

Figure 5.1 Design ranges, system ranges, and common ranges

5.2 Computing Information Content of Redundant Designs

A design is redundant if the number of DPs is larger than the number of FRs, and its design equation can be expressed as [Suh, 2001]

$$\{FR\} = [A]\ \{DP\} + [B]\{DP\}^{extra} \tag{5.6}$$

where {DP} is the vector of the primary DPs that are chosen to satisfy all FRs, and has the same dimension as {FR}; $\{DP\}^{extra}$ is the vector of the extra or redundant DPs that are left over after {DP} is chosen to satisfy {FR}; [*A*] is the square design

matrix that relates {DP} to {FR}; and [*B*] is the extra matrix that gives the effect of the extra DPs on FRs. According to Suh [2001], to satisfy the Independence Axiom, [*A*] must be either diagonal or triangular, but [*B*] can be any matrix, including a full matrix. In [Suh, 2001], Suh also presented a method to reduce information content of redundant designs by fixing the values of the extra DPs. This method does provide an effective way to eliminate the extra DPs as possible sources of random variation, thereby reducing information content. However, this method does not provide a method to compute the information content of redundant designs. In addition, it is noted that in many design practices, the values of the extra DPs cannot always be fixed. System temperature and process parameters (e.g. the fluid volume left in the syringe in the dispensing process) are a few examples of such DPs, and their random variations can cause the change in FRs. Therefore, design must be performed to accommodate these DPs' variations. Meanwhile for such a redundant design, computing its information content should be different from the one reviewed in the preceding section. Based on the definition of information content, an algorithm is presented in this section to compute the information content of redundant designs.

Consider a special case of Equation (5.6) – a redundant design that has two FRs and four uniformly distributed DPs, represented by

$$\begin{Bmatrix} \mathrm{FR}_1 \\ \mathrm{FR}_2 \end{Bmatrix} = \begin{bmatrix} A_{11} & 0 \\ A_{21} & A_{22} \end{bmatrix} \begin{Bmatrix} \mathrm{DP}_1 \\ \mathrm{DP}_2 \end{Bmatrix} + \begin{bmatrix} B_{11} & B_{12} \\ B_{21} & B_{22} \end{bmatrix} \begin{Bmatrix} \mathrm{DP}_3 \\ \mathrm{DP}_4 \end{Bmatrix} \tag{5.7}$$

In the above equation, if A_{21}=0 then the design is uncoupled, otherwise decoupled. Under the assumption that the design is linear (i.e., the elements of [A] and [B] are all constants), the extreme value of the variation in each FR due to the random variations in DPs can be derived from the above equation and given by

$$\chi \mathrm{FR}_i = \left|A_{ii}\delta \mathrm{DP}_i\right| + \sum_{j=1}^{2}\left|B_{ij}\delta \mathrm{DP}_{j+2}\right|, \qquad \{i\} = \{1,2\} \qquad \text{for an uncoupled design} \tag{5.8}$$

or

$$\chi \mathrm{FR}_i = \sum_{j=1}^{i}\left|A_{ij}\delta \mathrm{DP}_j\right| + \sum_{j=1}^{2}\left|B_{ij}\delta \mathrm{DP}_{j+2}\right|, \qquad \{i\} = \{1,2\} \qquad \text{for a decoupled design} \tag{5.9}$$

From the above equations, it can be seen that for both uncoupled design and decoupled design, the system range consists of two parts; one part is caused by the variation of the primary DPs and the other part by the variation of the redundant DPs. Graphically, the system ranges of both uncoupled design and decoupled design are illustrated in Figure 5.2. In particular, the parallelogram, which is denoted by vertices (1), (2), (3), and (4), represents the FR change caused by the variation of the redundant DPs; and the filled area represents the FR change caused by the variation of the primary DPs. Specifically, the coordinates of the four vertices of the parallelogram can be expressed as, based on Equations (5.8) or (5.9).

$$\begin{aligned}
&\text{vertex (1)}: (\left|B_{11}\delta \mathrm{DP}_3\right| + \left|B_{12}\delta \mathrm{DP}_4\right|, \ \left|B_{21}\delta \mathrm{DP}_3\right| + \left|B_{22}\delta \mathrm{DP}_4\right|)\\
&\text{vertex (2)}: (-\left|B_{11}\delta \mathrm{DP}_3\right| + \left|B_{12}\delta \mathrm{DP}_4\right|, \ -\left|B_{21}\delta \mathrm{DP}_3\right| + \left|B_{22}\delta \mathrm{DP}_4\right|)\\
&\text{vertex (3)}: (-\left|B_{11}\delta \mathrm{DP}_3\right| - \left|B_{12}\delta \mathrm{DP}_4\right|, \ -\left|B_{21}\delta \mathrm{DP}_3\right| - \left|B_{22}\delta \mathrm{DP}_4\right|)\\
&\text{Vertex (4)}: (\left|B_{11}\delta \mathrm{DP}_3\right| - \left|B_{12}\delta \mathrm{DP}_4\right|, \ \left|B_{21}\delta \mathrm{DP}_3\right| - \left|B_{22}\delta \mathrm{DP}_4\right|)
\end{aligned} \tag{5.10}$$

And the FR change due to the variation of the primary DPs, denoted by u_1 and u_2 for an uncoupled design and d_1, d_2, and d_3 for a decoupled design, as illustrated in Figure 5.2, are given by

$$\begin{aligned} u_1 &= \left|A_{11}\delta \mathrm{DP}_1\right| \\ u_2 &= \left|A_{22}\delta \mathrm{DP}_2\right| \end{aligned} \qquad \text{for an uncoupled design} \qquad (5.11)$$

or

$$\begin{aligned} d_1 &= \left|A_{11}\delta \mathrm{DP}_1\right| \\ d_2 &= \left|A_{21}\delta \mathrm{DP}_1\right| + \left|A_{22}\delta \mathrm{DP}_2\right| \\ d_3 &= -\left|A_{21}\delta \mathrm{DP}_1\right| + \left|A_{22}\delta \mathrm{DP}_2\right| \end{aligned} \qquad \text{for a decoupled design} \qquad (5.12)$$

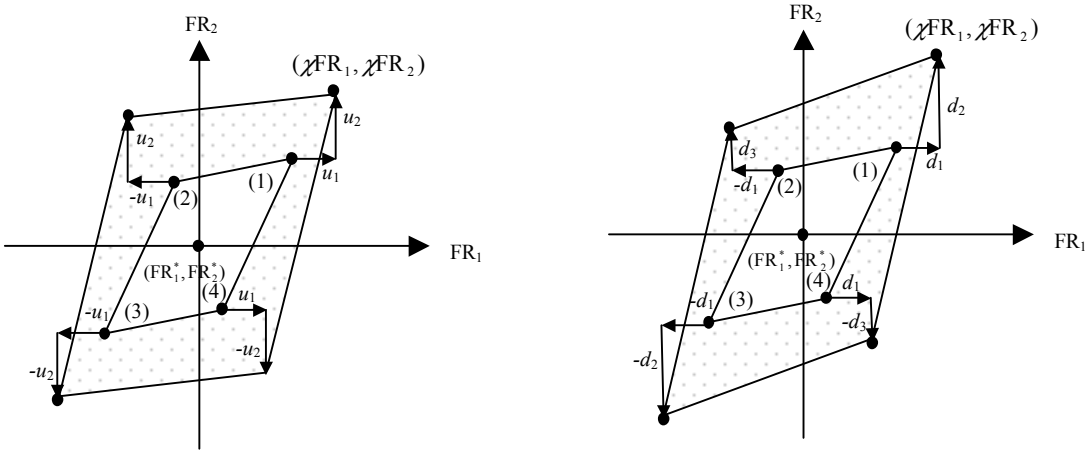

(a) uncoupled design (b) decoupled design

Figure 5.2 System ranges of redundant designs

From Equation (5.10), it is clear that the parallelogram is symmetrical about the targeted values $(\mathrm{FR}_1^*, \mathrm{FR}_2^*)$. Particularly, if [$B$] is a null matrix (i.e., the elements of [B] are all zeros) or the values of the extra DPs are fixed (i.e., both $\delta \mathrm{DP}_3$ and $\delta \mathrm{DP}_4$ are zeros), the parallelogram will reduce to the point of $(\mathrm{FR}_1^*, \mathrm{FR}_2^*)$.

In such a case, the system ranges for both uncoupled design and decoupled design illustrated in Figure 5.2 will be the same as the ones in Figure 5.1.

Once the system range is determined, the common range that is the intersection of the system range and the design range can be evaluated. Eventually, based on Equations (5.2) and (5.3), the information content of a redundant design can be calculated. It should be noted that, although the above algorithm is presented for the case where a redundant design has two FRs and four DPs for facilitating graphical illustration, it can be readily extended and applied to the design that has different number of FRs or DPs. To do so, Equations (5.8) and (5.9) should be changed in accordance with the number of FRs and the number of DPs, i.e.,

$$\chi \mathrm{FR}_i = \left| A_{ii} \delta \mathrm{DP}_i \right| + \sum_{j=1}^{n-m} \left| B_{ij} \delta \mathrm{DP}_{j+m} \right|, \qquad \{i\} = \{1, 2, \cdots, m\} \quad \text{for an uncoupled design} \tag{5.13}$$

$$\chi \mathrm{FR}_i = \sum_{j=1}^{i} \left| A_{ij} \delta \mathrm{DP}_j \right| + \sum_{j=1}^{n-m} \left| B_{ij} \delta \mathrm{DP}_{j+m} \right|, \qquad \{i\} = \{1, 2, \cdots, m\} \quad \text{for a decoupled design} \tag{5.14}$$

where m is the number of FRs and n is the number of DPs.

5.3 Evaluation of the Designs of Fluid Dispensing Systems

5.3.1 Review of Models of Dispensing Systems

Figure 5.3 shows the main parts of the three dispensing systems discussed previously and their manipulated parameters, i.e., the supplied air pressure (P) in

time-pressure dispensing, the screw angular speed (ω) in rotary-screw dispensing, and the piston movement speed ($\dot{X}$) in positive-displacement dispensing. In the present study, it is assumed that the fluid being dispensed is Newtonian for simplification, and that the fluid viscosity (η) is related to temperature (T) by

$$\eta = Ke^{\frac{T_k}{T}} \tag{5.15}$$

where K and T_k are the coefficients associated. For a given fluid, the values of K and T_k are determined experimentally.

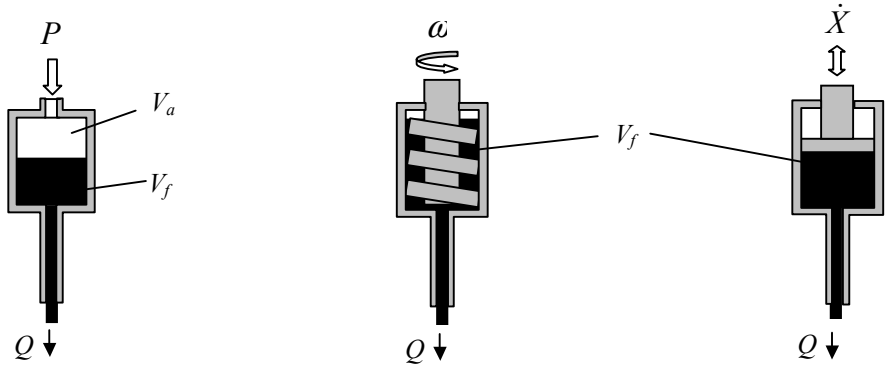

(a) time-pressure (b) rotary-screw (c) positive-displacement

Figure 5.3 Dispensing systems and their manipulated parameters

Generally, the development of a model for a dispensing system consists two parts: representing the fluid pressure at the syringe bottom and representing the flow rate in the needle. To represent the fluid pressure at the syringe bottom, it is assumed for the time-pressure dispensing system that (1) only the compressibility of air is considered by neglecting that of fluid, considering that air is much easier to be compressible than fluid and (2) the friction loss of the fluid flow in the syringe

can be ignored, which implies the fluid pressure in the syringe is uniform and equal to the air pressure in the syringe. Under these assumptions, the fluid pressure at the syringe bottom, P_s, is governed by the following equations [Chen *et al*., 2002]:

$$\dot{m} = \frac{C_m C_d A_o P}{\sqrt{T}} \tag{5.16}$$

$$\frac{dP_s}{dt} = \frac{\gamma R T}{V_a} \dot{m} \tag{5.17}$$

where $\dot{m}$ is the mass flow rate through the orifice connected to the syringe, A_o the area of air flow passage of the orifice, T the system temperature, γ the ratio of the specific heats (1.4 for air), R a constant (287 J/kg/K for air), V_a the volume of air in the syringe as shown in Figure 5.3 (note that V_a is not a constant but increases with the dispensing process proceeding), C_d the discharge coefficient, and C_m the mass flow parameter and given by

$$C_m = \begin{cases} 0.0405 & \text{if } \frac{P_s}{P} < 0.528 \\ \sqrt{\frac{2\gamma}{R(\gamma-1)}\left[\left(\frac{P_s}{P}\right)^{\frac{2}{\gamma}} - \left(\frac{P_s}{P}\right)^{\frac{\gamma+1}{\gamma}}\right]^{\frac{\gamma+1}{\gamma}}} & \text{if } \frac{P_s}{P} \geq 0.528 \end{cases} \tag{5.18}$$

For the rotary-screw dispensing system shown in Figure 5.3(b), it is assumed that (1) the fluid is compressible; and (2) the fluid pressure is linearly distributed in down channel direction. The fluid pressure at the syringe bottom is then governed by [Hashemi, 2006]:

$$C_\omega \omega - Q = \frac{V_f}{2B}\frac{dP_s}{dt} + C_p(P_s - P_t) \tag{5.19}$$

where Q is the flow rate of fluid out of the syringe, V_f the fluid volume in the syringe as shown in Figure 5.3 (b) (note that V_f decreases with the dispensing process proceeding), B the fluid bulk modulus, P_t the fluid pressure at the top of the syringe, C_ω the coefficient associated with the pure drag flow (i.e., the flow without a pressure gradient in down channel direction), and C_p the coefficient associated with the pure pressure-driven flow (i.e., the flow without relative motion between the screw and the syringe). Both C_ω and C_p are dependent on the geometry of rotary screw (as shown in Figure 5.4) and the fluid viscosity, which are given by [Rauwendaal, 2004]

$$C_\omega = \frac{WHD_{sw}\cos\phi}{4} \tag{5.20}$$

$$C_p = \frac{WH^3}{12\eta L_c} \tag{5.21}$$

in which W is the cross channel width, H the channel depth, D_{sw} the inside diameter of the syringe, ϕ the helix angle of the screw, and L_c the length of fluid in down channel direction.

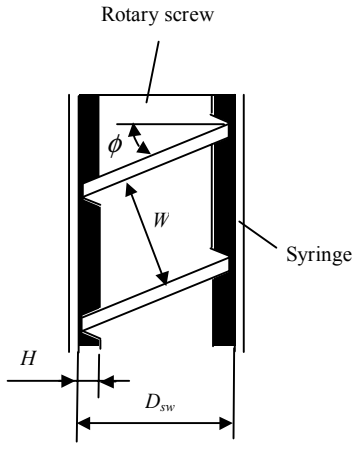

Figure 5.4 Geometry of a rotary screw

For the positive-displacement dispensing system shown in Figure 5.3 (c), it is assumed that (1) the fluid is compressible and (2) the friction loss of the fluid flow in the syringe is ignored, which implies the fluid pressure in the syringe is uniform. The fluid pressure at the syringe bottom is then governed by [Chen and Kai, 2004]

$$A_p \dot{X} - Q = \frac{V_f}{\beta} \frac{dP_s}{dt} \tag{5.22}$$

where A_p is the cross-section area of the piston, and other symbols have the same meaning as mentioned previously.

To represent the flow rate in the needle, the following assumptions are made: (1) the fluid flow in the needle is fully developed and laminar; (2) there is no slip between fluid and the needle wall; and (3) the compressibility of the fluid in the needle is ignored given that the fluid volume in the needle is much smaller than that in the syringe, which also suggests the flow rate in the needle is equal to the one of the fluid dispensed. By neglecting the inertia of the fluid in the needle for simplification, the flow rate (Q) can be obtained by using the well-known Poiseuille equation:

$$Q = Q_u \left(P_s - P_e \right) \tag{5.23}$$

where p_e is the fluid pressure at the exit of needle, which is equal to the pressure of ambient air if ignoring the influence of fluid surface tension [Chen and Kai, 2004]; and Q_u is the flow rate under the action of a unit pressure and given by

$$Q_u = \frac{\pi D_n^{\,4}}{128 \eta L_n} \tag{5.24}$$

in which D_n and L_n are the inner diameter and length of the needle. It should be noted that Equation (5.23) represents the dynamics of the flow rate because P_s is a dynamic response to the manipulated parameter, as seen from Equations (5.17), (5.19), and (5.22). Once P_s reaches its steady-state value, the flow rate obtained from Equation (5.23) becomes the steady state one.

Once the flow rate of the fluid dispensed is determined, the amount of the fluid dispensed, M, can be obtained by using the following integration

$$M = \rho \int_0^{T_d} Q \, \mathrm{d}\, t \tag{5.25}$$

where ρ is the fluid density and T_d is the time period of dispensing. T_d is determined by the duration of pressurized air in time-pressure dispensing, the duration of the screw rotation in rotary-screw dispensing, or the duration of the piston movement in positive-displacement dispensing.

5.3.2 Axiomatic Evaluation of Dispensing Systems

Based on the previous models, an evaluation of the designs of fluid dispensing systems is presented here by means of axiomatic design principles. The fluid properties and the main parameters of the dispensing systems, used in this evaluation, are listed in Table 5.1. Most of the values were taken or adapted from the previous studies [Chen and Kai, 2004; Chen *et al*., 2002; Hashemi, 2006].

Table 5.1 Fluid properties and main parameters of dispensing systems

	Parameters	Values
Fluid properties	Viscosity, η	$\eta = 25.39e^{\frac{92.47}{T}}$ Pa · s
	Density, ρ	950.0 Kg/m^3
	Bulk modulus, B	1.0×10^9 Pa
Common parameters for the three systems	Syringe capacity	60 cc
	Needle diameter, D_n	1.3 mm
	Needle length, L_n	18.0 mm
	Fluid pressure at the exit of needle, P_e	1.0×10^5 Pa
Time-pressure dispensing system	Effective area, C_dA_o	1.2×10^{-6} m^2
Rotary-screw dispensing system	Inside diameters of syringe, D_{sw}	25.0 mm
	Channel depth, H	4.0 mm
	Cross channel width, W	22.96 mm
	Helix angle of the screw, ϕ	17 degrees
	Fluid pressure at the top of syringe, P_t	1.0×10^5 Pa
Positive-displacement dispensing system	Piston diameter	25.0 mm

Depending on its applications, the requirements imposed on a dispensing system may vary. For continuous dispensing such as the application in the die encapsulation shown in Figure 5.5(a), the steady state flow rate of the fluid dispensed must be controlled accurately in order to achieve the desired profile of dam or the desired amount of the fluid required to fill the dam inside. For discontinuous dispensing such as the application in the surface mount technology shown in Figure 5.5(b), the amount of the fluid dispensed must be controlled precisely in order to secure the component with high degrees of quality and reliability.

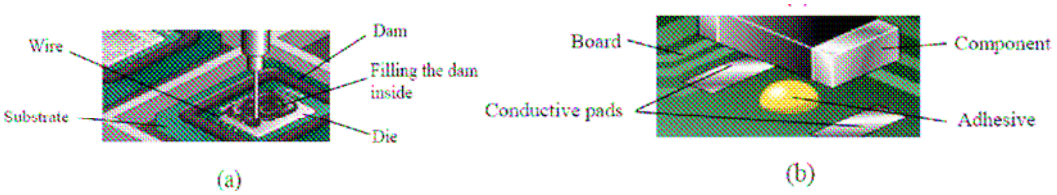

Figure 5.5 Dispensing applications
(a) die encapsulation and (b) surface mount technology

Thus, the functional requirements of dispensing systems may be set as the steady state flow rate and the amount of the fluid dispensed. In particular, in this study their targeted values and tolerance are specified as follows:

FR_1 = dispense fluid at a steady state flow rate of 10.0 mg/s with a tolerance of ± 2%

FR_2 = dispense a fluid amount of 4.0 mg with a tolerance of ± 1%

The magnitude and duration of the manipulated parameter (*i.e.*, the air pressure in time-pressure dispensing, the screw angular speed in rotary-screw dispensing, or the piston movement speed in positive-displacement dispensing) are chosen to satisfy the above FRs; meanwhile the system temperature and the fluid volume in the syringe are considered as the redundant DPs because both of them can affect, but are not chosen to satisfy, the above FRs.

DP_1 = the magnitude of manipulated parameter, M_c.

DP_2 = the duration of manipulated parameter, T_c.

DP_3 = the system temperature, T.

DP_4 = the fluid volume in the syringe, V_f (note that for time-pressure dispensing, V_f is equal to the syringe capacity minus the air volume in the syringe, as shown in Figure 5.3(a)).

In order to place the FRs on their targeted values, the nominal DP values need to be determined. In industrial fields, the system temperature (*i.e.*, DP_3) is usually specified based on the recommendation from the supplier of the fluid being dispensed in order to minimize the air entrapment in the dispensing process. In this study, the nominal value of DP_3 is set as 50°C. As for the fluid volume in the syringe (*i.e.*, DP_4), since it is not a constant but decreases continuously with the dispensing process proceeding, a half of the syringe capacity is used as the nominal value of DP_4. Once DP_3 and DP_4 are determined, the nominal values of DP_1 and DP_2 (*i.e.*, the magnitude and duration of P in the time-pressure dispensing system, the magnitude and duration of ω in the rotary-screw dispensing system, or the magnitude and duration of $\dot{X}$ in the positive-displacement dispensing system) can be determined based on the models presented in the preceding section in order to place the FRs on their targeted values. The determined nominal values of all DPs are listed in Table 5.2.

Table 5.2 Nominal values and variations of the DPs of dispensing systems

		Time-pressure	Rotary-screw	Positive-displacement
Magnitude (DP_1)	Nominal Value	3.79×10^{5} Pa	2.57 rad/s	2.14×10^{-2} mm/s
	Variation	$\pm 1\times10^{3}$ Pa	$\pm 1\times10^{-2}$ rad/s	$\pm 1\times10^{-4}$ mm/s
Duration (DP_2)	Nominal Value	383 ms	400 ms	400 ms
	Variation	$\pm 2\% \cdot DP_2$		
System Temperature (DP_3)	Nominal Value	$50^{o}C$		
	Variation	$\pm 2^{o}C$		
Fluid volume in syringe (DP_4)	Nominal Value	30 cc	15.8* cc	30 cc
	Variation	$\pm$ 30 cc	$\pm 2\% \cdot DP_4$	$\pm$ 30 cc

* 15.8 cc is evaluated given that the fluid volume in syringe is a half of the space between the syringe and the screw.

At these nominal values, the design matrix [*A*] and the extra matrix [*B*] were then evaluated numerically, and the results are given in Table 5.3. It can be seen that all of the design matrixes are triangular. Therefore, the three designs of dispensing system are all decoupled. In other words, each of the FRs can be satisfied if the DPs are determined in a proper sequence, i.e., adjusting the magnitude of the manipulated parameter (DP_1) to achieve the desired steady state flow rate (FR_1) and adjusting the duration of the manipulated parameter (DP_2) to achieve the desired amount (FR_2). In addition, the magnitudes of the extra matrix elements suggest that the system temperature (DP_3) and the fluid volume in syringe (DP_4) have varying effects on FRs, depending on the dispensing systems. In particular, the system temperature (DP_3) has more significant effect on the two FRs in time-pressure dispensing than in positive-displacement dispensing; and that the fluid volume in the syringe (DP_4) can affect the amount of fluid dispensed (FR_2) the most significantly in rotary-screw dispensing, nevertheless it does not affect the steady-state flow rate (FR_1) in both time-pressure and positive-displacement dispensing.

Table 5.3 Design matrix [*A*] and extra matrix [*B*] of dispensing systems

	[*A*]	[*B*]
Time-pressure	$\begin{vmatrix} 2.63\times10^{-5}\ \frac{\text{mg/s}}{\text{Pa}} & 0 \\ 1.28\times10^{-5}\ \frac{\text{mg}}{\text{Pa}} & 9.70\times10^{-3}\ \frac{\text{mg}}{\text{ms}} \end{vmatrix}$	$\begin{vmatrix} 3.70\times10^{-1}\ \frac{\text{mg/s}}{^{\circ}\text{C}} & 0 \\ 1.50\times10^{-1}\ \frac{\text{mg}}{^{\circ}\text{C}} & 5.00\times10^{-3}\ \frac{\text{mg}}{\text{cc}} \end{vmatrix}$
Rotary-screw	$\begin{vmatrix} 3.88\ \frac{\text{mg/s}}{\text{rad/s}} & 0 \\ 1.55\ \frac{\text{mg}}{\text{rad/s}} & 0.01\ \frac{\text{mg}}{\text{ms}} \end{vmatrix}$	$\begin{vmatrix} 0 & 6.27\times10^{-1}\ \frac{\text{mg/s}}{\text{cc}} \\ 0 & 2.51\times10^{-1}\ \frac{\text{mg}}{\text{cc}} \end{vmatrix}$
Positive-displacement	$\begin{vmatrix} 4.66\times10^{2}\ \frac{\text{mg/s}}{\text{mm/s}} & 0 \\ 1.86\times10^{2}\ \frac{\text{mg}}{\text{mm/s}} & 0.01\ \frac{\text{mg}}{\text{ms}} \end{vmatrix}$	$\begin{vmatrix} 0 & 0 \\ 7.48\times10^{-4}\ \frac{\text{mg}}{^{\circ}\text{C}} & -1.00\times10^{-3}\ \frac{\text{mg}}{\text{cc}} \end{vmatrix}$

Now, let's consider the information content of the designs of dispensing systems. To do this, the variations of all DPs are specified based on the specifications of typical commercial dispensing systems and also given in Table 5.2. In addition, it is assumed in this study that all of the DPs are uniformly distributed and that the dispensing performance is linear within the design ranges. This linear assumption would safely be made because, as a fact, the magnitude and duration of the manipulated parameter (i.e., DP_1 and DP_2) and the system temperature (DP_3) are controlled in dispensing systems and their variations are typically very small. Although the fluid volume in the syringe (DP_4) can vary from full to empty in a dispensing process by using a time-pressure or positive-displacement dispensing system, the authors' previous studies [Chen and Kai, 2004; Chen *et al*., 2002] revealed that the fluid volume has nearly linear effect on dispensing. Under the above assumptions, the system range of each dispensing system can then be evaluated by using Equation (5.9). The results are shown graphically in Figure 5.6, along with the design ranges. The common ranges were then evaluated based on the geometry given in Figure 5.6. Eventually, the probability and information content of each dispensing system were calculated from Equations (5.2) and (5.3), and the results are summarized in Table 5.4. It can be seen that the positive-displacement system has the minimum information content. Based on the Information Axiom, it can be concluded that the positive-displacement is the best design and then followed by the rotary-screw dispensing system and the time-pressure dispensing system. In other words, the positive-displacement system has the most accurate dispensing performance; and the performance of the time-pressure system, by contrast, is the most sensitive to the variation of DPs. It should be noted that although the evaluation presented in this

section was carried out for existing dispensing systems, the method used can also be extended and applied for the design and development of new dispensing systems.

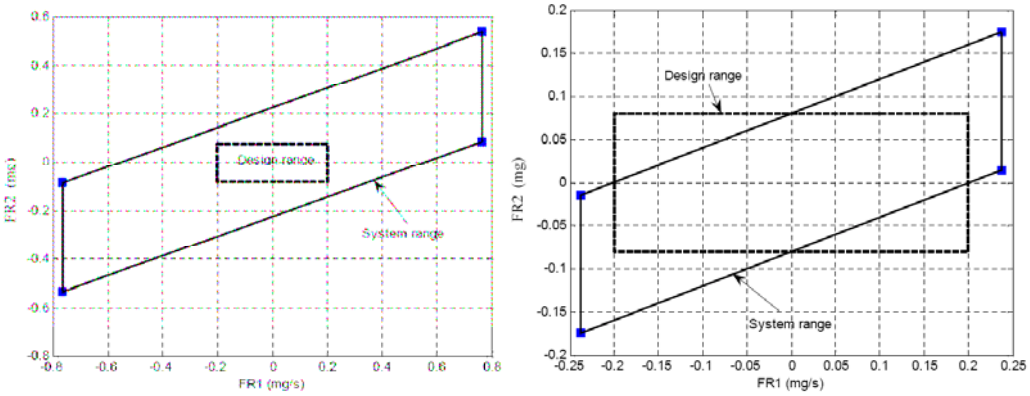

(a) time-pressure (b) rotary-screw

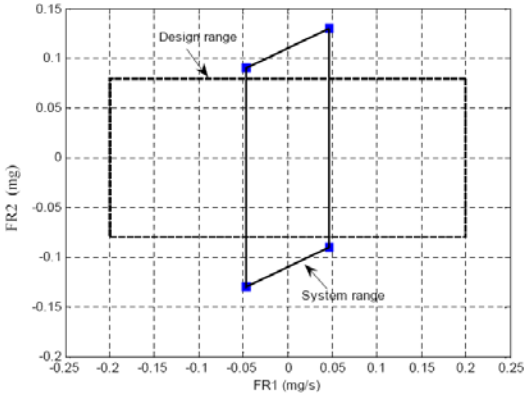

(c) positive-displacement

Figure 5.6 System ranges and design ranges of dispensing systems

Table 5.4 Probability and information content of dispensing systems

	Time-pressure	Rotary-screw	Positive-displacement
Probability of success (%)	9.93	42.13	71.80
Information content (bits)	3.422	1.247	0.478

5.4 Summary

This chapter presents an evaluation on the designs of dispensing systems by means of the Independence Axiom and the Information Axiom. First, an algorithm is developed for computing the information content of redundant designs. In the algorithm, the change in FRs is divided into two parts: one part from the variation of the primary DPs and the other part from the variation of the redundant DPs. This enables one readily to evaluate the system range of a redundant design and to calculate its information content. Second, it is illustrated in this chapter that existing designs of fluid dispensing systems are all redundant if taking into account the influence of system temperature and the influence of the fluid volume left in the syringe. Also, it was shown that existing designs of fluid dispensing systems are all decoupled. This suggests that the independence of FRs can be satisfied by determining DPs in a proper sequence. Eventually, the information content of existing dispensing system, calculated by using the aforementioned algorithm, shows that the positive-displacement system is the best design, followed by the rotary-screw dispensing system and then the time-pressure dispensing system. This is consistent with what has been recognized in industry based on experiments.

6. CONCLUSIONS AND FUTURE WORK

6.1 Conclusions

Fluid dispensing is a complex process due to the involvement of the compressibility of fluid and non-Newtonian behaviour of the dispensed fluid. As a result, the design and modeling of dispensing systems becomes a challenging task, which is an interdisciplinary area involving polymer material engineering, non-Newtonian fluid mechanics, electronics packaging, and simulations. This thesis presents a comprehensive study on the modeling of the positive displacement dispensing system and an integrated approach for the design of fluid dispensing systems based on the independence axiom and the information axiom. The main contributions of the research are summarized as follows:

1. For the characterization of the rheological behaviour of fluids for electronics packaging, various equations such as power-law and 3-parameter Carreau model are reviewed and examined in this research. Based on the previous experiments on the fluid Hysol FP4451, a 3-parameter Carreau model for the fluid is derived for use in the present study.

2. A dynamic model that represents the flow rate of fluid dispensed is developed. Based on the model, the effects of factors such as the dispensing time, fluid level in the syringe, fluid flow behaviour, fluid temperature, and fluid

compressibility on the flow rate are investigated. Simulation results show that the flow rate of fluid dispensed can be described by a second order system. Because of the dynamics of the flow rate, the volume of fluid dispensed is different from the volume displaced by the piston motion. This difference indicates that the positive-displacement approach is not truly volumetric dispensing if the fluid amount dispensed is very small.

3. To calculate the fluid amount on a board, a model based on the non-Newtonian liquid bridge breaking criterion is developed under the assumption that extensional viscosity has a linear relationship with shear viscosity if the extensional strain is minute or the breaking time is short. A simulation study was carried out based on the model developed. According to the simulation results, it was found that both surface tension and initial fluid amount dispensed out of the needle affect the fluid amount transferred onto the board. Specifically, for surface tension, the greater surface tension, the less fluid stays on the board; and for the initial fluid amount dispensed, the greater initial fluid amount, the more fluid stays on the board. However, from the simulation results given in the present study, it is also seen that the change of the final fluid on the board in terms of percentage of the board mass to the initial mass is quite limited.

4. To evaluate the designs of different dispensing systems, an algorithm was developed to compute the information content of redundant designs and an evaluation by means of the Independence Axiom and the Information Axiom is

carried out. It is illustrated that existing designs of fluid dispensing systems are all redundant and decoupled. Also, it is illustrated from the calculated information content of existing dispensing systems that the positive-displacement system is the best design, followed by the rotary-screw dispensing system, and then the time-pressure dispensing system.

6.2 Future works

There are a number of issues that arise from the present study and may need to be further addressed. For this purpose, the following recommendations are suggested for the future work.

1. Experimental verification of the model developed for of the flow rate dynamics

The model to represent the dynamic flow rate in the positive displacement dispensing process was developed in this research. Its experimental verification, however, was not possible due to the time and instrument limitations. In the future, experiments are recommended to be conducted. Specifically, the fluid is dispensed under various operation conditions; and the fluid amount dispensed is measured, which is in turn used to determine the flow rate. The effectiveness of the model developed is then to be illustrated by comparing the measured flow rates and the simulated ones from the model.

2. Theoretical and experimental studies on the deformation of non-Newtonian fluids in a liquid bridge with disks of different radii

The model developed in the present study is based on the assumptions that extensional strain is minute and deformation time is short. Therefore, the extensional viscosity is linearly related to the shear viscosity under the same scale shear rate. However, the real deformation time is possibly longer than what it is assumed in the present study. This means, instead of the existence of a linear relationship with shear viscosity, the constitutive equation of the extensional viscosity may become non-linear to the extension strain. Meanwhile, in the extension experiments used to investigate the deformation behaviours of non-Newtonian liquid bridge, it is always assumed that the top and bottom plates are identical, which is not the situation in the present study. To solve this problem, a 3-step method was developed in the present research and its effectiveness was illustrated by simulations. As an extension study of the present one, further studies on the extensional deformation of a non-Newtonian liquid bridge are suggested, which may include (1) the development of the constitutive equation of extensional viscosity of FP4451 used in the dispensing process if the extension strain goes beyond the range considered in the present study and (2) the implementation of the experimental study on the extensional deformation of the FP4451 liquid bridge that is confined by two plates with unequal radii.

REFERENCES

[1] Babiarz, A. J., *et al*., 1999, "Cavity Down BGA Flip Chip SCM/MCM BGA Assembly Processs for Accurate Fluid Dispensing," *Asymtek technical report: http://www.asymtek.com*

[2] Babiarz, A.J., 1999, "Die Encapsulation and Flip Chip Underfilling Process for Area Arry Packaging of Advanced Integrated Circuits," *Asymtek technical report: http://www.asymtek.com*

[3] Barnes, H.A., Hutton, J.F., and Walters, K., 1989, *An Introduction to Rheology,* Elsevier Science Publishers B.V., pp. 18, 80-81.

[4] Chen, X.B., 2002, "Modeling and Off-Line Control of Fluid Dispensing for Electronics Packaging," *Ph.D. Dissertation*, University of Saskatchewan.

[5] Chen, X.B., Schoenau, G., and Zhang, W.J., 2000, "Modeling of Time-Pressure Fluid Dispensing Processes," *IEEE Transactions on Electronics Packaging Manufacturing*, vol. 23, pp. 300-305.

[6] Chen, X.B., Schoenau, G., and Zhang, W.J., 2002 "On the Flow Rate Dynamics in Time-Pressure Dispensing Processes," *ASME Journal of Dynamic Systems, Measurement, and Control*, vol. 124, pp. 693-698.

[7] Chen, X. B., Zhang, W. J., Schoenau, G., and Surgenor, B., 2003, "Off-Line Control of Time-Pressure Dispensing Processes for Electronic Packaging," *IEEE Trans. on Electronics Packaging Manufacturing*, vol. 26, pp. 286-293.

[8] Chen, X. B. and Kai, J., 2004, "Modeling of Positive-Displacement Fluid Dispensing Processes," *IEEE Trans. On Electronics Packaging Manufacturing*, vol. 27, pp. 157-163.

[9] Chen, X.B., 2007, "Modeling of Rotary Screw Fluid Dispensing Processes," *Journal of Electronic Packaging*, vol. 29, pp. 172-178.

[10] Dixon, D., Kazalski, J., Murch, F., and Marongelli, S., 1997, "Practical Issues Concerning Dispensing Pump Technologies," *Circuits Assembly*, August, pp. 36-40.

[11] Espino, J.L., Meseguer J., and Simavilla, A.L., 2002, "An Experimental Study of The Breakage of Liquid Bridges at Stability Limit of Minimum Volume," *Physics of Fluids*, vol. 14, Number 10, pp. 3710-3713.

[12] Frey, D. D., Jahangir, E. J., and Engelhardt, F., 2000, "Computing the Information Content of Decoupled Designs," *Research in Engineering Design*, Vol. 12, pp. 90-102.

[13] Gaudet, S. and Mckinley, G.H., 1998, "Extensional Deformation of Non_Newtonian Liquid Beidges," *Computational mechanics*, vol. 21, pp. 461-476

[14] Han, S. and Wang, K. K., 1997, "Analysis of the Flow of Encapsulant during Underfill Encapsulation of Flip-chips," *IEEE Trans. on Components, Packaging, and Manufacturing Technology - Part B*, vol. 20, pp. 424-433.

[15] Hashemi, M., 2006, "Modeling of the Rotary-Screw Dispensing System," *M.Sc. Thesis*, University of Saskatchewan, Saskatoon, Canada.

[16] Hingmann, R. and Marczinke, B. L., 1994, "Shear and Elongational Flow Properties of Polypropylene Melts," *Journal of Rheology*, vol. 38, pp. 573-587.

[17] Hong, Y. P. and Li, H. X, 2003, "Comparative Study of Fluid Dispensing Modeling," *IEEE Trans. on Electronics Packaging Manufacturing*, vol. 26, pp. 273-280.

[18] Hsu, T.R., 2004, *MEMS Packaging*, *INSPEC*, London, United Kingdom.

[19] James F. S., 1996, *Rheological methods in Food Process Engineering*, Freeman Press.

[20] Jeans, E., 1997, "Nonlinear Dynamics and Breakup of Free-Surface Flows," *Reviews of Modern Physics*, Vol. 69, pp. 865-930.

[21] Joshi, Y.M. and Denn, M.M., 2003, "Rupture of Entangled Polymeric Liquids in Elongational Flow," *Journal of Rheology*, vol. 47 pp. 291-298.

[22] Joshi, Y.M. and Denn, M.M., 2004, "Failure and Recovery of Entangled Polymer Melts in Elongational Flow," *Rheology Reviews 2004*, pp. 1-17.

[23] Landers, R., Pfister, A., Hubner, U., John, H., Schmelzeisen, R., and Mulhaupt, R., 2002 "Fabrication of Soft Tissue Engineering Scaffolds by Means of Rapid Prototyping Techniques," *Journal of Materials Science*, vol. 37, pp. 3107-3116.

[24] Lewis, A., Adamson, S., Nielsen, L. M., and Ryan, L., 2003 "Fluid Dispensing Capabilities for Assembly of MEMES," *The Workshop on MEMS Sensor Packaging*, Delta Denmark.

[25] Malkin A.Y. and Petrie, C.J.S., 1997, "Some Conditions for Rupture of Polymer Liquids in Extension," *Journal of Rheology,* vol. 41, pp. 1-25.

[26] McKinley, G.H. and Hassager, O., 1999, "The Considere Condition and Rapid Stretching of Linear and Branched Polymer Melts," *Journal of Rheology*, vol. 43, pp. 1195-1211.

[27] McKinley, G.H. and Sridhar, T., 2002, "Filament-Stretching Rheometry of Complex Fluids," *Annual Review of Fluid Mechanics*, vol. 34, pp. 375-415.

[28] Merritt, H.E., 1967, *Hydraulic Control Systems*, John Wiley & Sons, Inc.

[29] Meseguer, J., 1983, "The Influence of Axial Microgravity on The Breakage of Axisymmetric Slender Liquid Bridges," *Journal of Crystal Growth,* vol. 61, pp. 577-586.

[30] Meseguer, J., 1983, "The Breaking of Asisymmetric Slender Liquid Bridges," *Journal of Fluid Mechanics*, vol. 130, pp.123-151.

[31] Meseguer, J., 1984, "Stability of Slender, Axisymmetric Liuiqd Bridges between Unequal Disks," *Journal of Crystal Growth,* vol. 67, pp. 141-143.

[32] Meseguer, J. and Espino, J.L., 2003, "On the Breaking of Long, Axisymmetric Liquid Bridges between Unequal Supporting Disks at Minimum Volume Stability Limit," *European Journal of Mechanics B/Fluids,* vol. 22, pp. 355-368.

[33] Meseguer, J., Perales, J.M., Martinez, I., Bezdenejnykh, N.A., & Sanz, A., 1999, "Hydrostatic Instability in Floating Zone Crystal Growth Process," *European Journal of Crystal Growth*, vol. 5, pp. 27-42.

[34] Nakayama, T., Niwa, E., and Hamada, I., 1980, "Pipe transportation of minced fish paste," *Journal of Food Science*, vol. 45, pp. 844-847.

[35] Ness, C.Q. and Lewis, A.R., 1998, "Adhesives/Epoxies & Dispensing," *Surface Mount Technology (SMT)*, May, pp. 114-122.

[36] Okada, F. and Larsen, M., 2004, "Adhesives/Epoxies & Dispensing," *Report on Surface Mount Technology, Liquid control Corp,.*

[37] Quinones, H. *et al*., 2003, "Fluid dispensing processes for next generation electronics," *Asymtek technical report: http://www.asymtek.com*

[38] Rauwendaal C., 1986, *Polymer Extrusion*, Hanser Gardner Publication, Inc.

[39] Rauwendaal, C., 2004, *Polymer Extrusion*, Hanser Gardner Publication, Inc.

[40] Razban, A., 1993, "Intelligent Control of An Automated Adhesive Dispensing Cell," *Ph.D. Dissertation*, Imperial College.

[41] Razban, A. and Davies, B. L., 1995, "Analytical Modeling of the Automated Dispensing of Adhesive Material," *Journal of Adhesion Science Technology*, vol. 9, pp. 1435-1450.

[42] Salmon, E., 1987, *Encapsulation Of Electronic Devices and Components*, Marcel Dekker, Inc.

[43] Skelland, A.H.P. 1967, *Non-Newtonian Flow and Heat Transfer*, John Wiley & Sons, Inc., pp. 2-3.

[44] Slobozhanin, L.A. and Meseguer, J., 1993, "Stability of Liquid Bridges between Equal Disks in An Axial Gravity Field," *Physics of Fluids A*, Vol. 5, pp. 1305-1314.

[45] Soron, E. and Babiarz, A., 1997, "Advanced IC Encapsulation Challenges: The Search for A True Positive Displacement Pump," *Asymtek technical report: http://www.asymtek.com*

[46] Spiegelberg, S.H. and McKinley, G.H., 1996, "The Extensional Theology of Non-Newtonian Materials," 3rd *Microgravity Fluid Physics Conference*, Cleveland, Ohio, pp. 377-382.

[47] Spiegelberg, S. H., Ables, D. C. and McKinley, G.H., 1996, "The Role of End-Effects on Measurements of Extensional Viscosity in Filament Stretching Rheometers," *Journal of Non-Newtonian Fluid Mechanics*, Vol. 64, pp. 229-267.

[48] Suh, N. P., 2001, *Axiomatic Design: Advances and Applications*, Oxford University Press, Inc.

[49] Wan, J.W., 2004, "Analysis and Modeling of Underfill Flow Driven by Capillary Action in Flip Chip Packaging," *Ph.D. Dissertation*, University of Saskatchewan.

[50] Wedekin, S., 2001, "Micro Dispensing Comes of Age," *Surface Mount Technology (SMT)*, April, pp. 62-71.

[51] Wong, C.P., 1998, "Polymers for Encapsulation: Materials Processes and Reliability," *Chip Scale Review*, vol. 2, pp. 30.

[52] Yang, L.Y., King, C.K., and Bernstein, J.B., 2003, "Liquid Dispensing Encapsulation in Semiconductor," *Microelectronics International*, vol. 20, pp. 29-35.

[53] Yao, M.W., McKinley, G.H., and Debbaut, B., 1998, "Extensional Deformation, Stress Relaxation and Necking Failure of Viscoelastic Filaments," *Journal of Non-Newtonian Fluid Mechanics*, vol. 79, pp. 469-501.

[54] Yao, M.W., Spiegelbag, S.H., and McKinley, G.H., 2000, "Dynamics of Weakly Strain-Hardening Fluids in Filament Stretching Devices," *Journal of Non-Newtonian Fluid Mechanics,* vol. 89, pp. 1-43.

[55] Yildirim, O.E. and Basaran, O.A., 2001, "Deformation and Breakup of Stretching Bridges of Newtonian and Shear-Thinning Liquids: Comparison of One-and Two-Dimensional Models," *Chemical Engineering Science* vol. 56, pp. 211-233.

[56] Zhang, X., Padgett. R.S, and Basaran O.A., 196, "Nonlinear deformation and breakup of stretching liquid bridges," *Journal of Fluid Mechanics,* vol. 329, pp. 207-245.

[57] Zhao, Y.X., *et al*., 2005, "Integrated Modeling of A Time-Pressure Fluid Dispensing System for Electronics Manufacturing," *The International Journal of Advanced Manufacturing Technology,* vol. 26, pp. 1-9.

APPENDIX

I. Simulink Block based on Equation (4.41) for calculating fluid amount transferred onto the board.

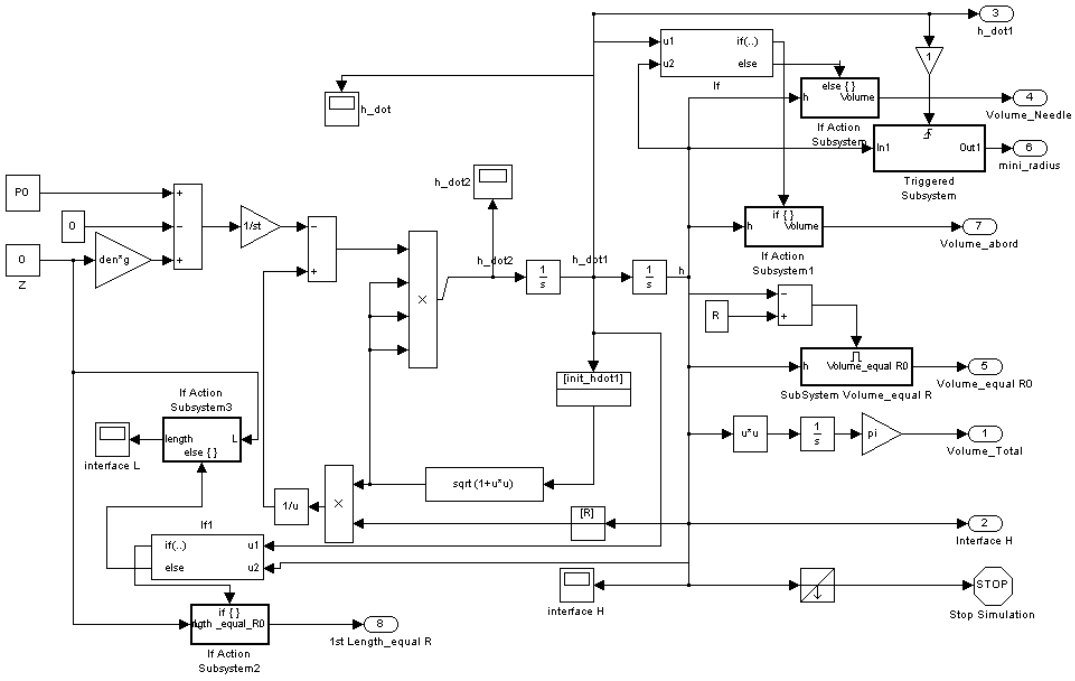

II. Program Code for simulating the bridge shape and fluid amount transferred onto the board

```
% Liquid bridge shape and fluid amount on board.m

% This program is used to determine the critical shape of the bridge between the needle and the
board and calculate the fluid amount on board.

%clc; clear; clf;

% 1. Given parameters
  R = 1.06/2/1000;                          % External Diameter of the Needle,m
  con_angle = - pi/3.3;                     % Initial contact angle needle, degree
  unit_angel = pi*0.5/180                   % step angle
  st  =    0.43;                            % Surface Tension, N/m
  den = 1780.0;                             % Density, Kg/m^3
  g  =9.8;                                  % Gravity Acceleration, m/s^2
  v_0 = 30/1000;                            % Elongation speed, 30mm/s

% 1.1 calculates the initial differential pressure in the midst of the needle & top plate

  deltaZ = 0.001/1000;                       % step displacement of Z in Z axial

  Volum_Z = (deltaZ * pi*(R^2+(R-deltaZ * tan(con_angle))^2+R*(R-deltaZ*tan(con_angle))))/3
                                             %  volume of the deltaZ distance to top plate


  force_z = den*g*Volum_Z                    % force of the volume_Z
  differencialV = Volum_Z- pi*R^2*deltaZ     % differencial volume of delta Z and pi*R^2*deltaZ

  initial_P0 =(force_z + 2*pi*R*den*g*tan(con_angle)*deltaZ^2-pi*R^2*den*g*deltaZ-
              2*pi*st*sin(con_angle)*tan(con_angle)*deltaZ-
              pi*den*g*deltaZ^3*(tan(con_angle))^2)/(pi*(deltaZ)^2*(tan(con_angle))^2-
              2*pi*deltaZ*R*(tan(con_angle)))

                                            % Initial differential pressure according to
                                             % static force balance considering
                                            % Gravity acceleration force.
  P0 = - st*sin(con_angle)/R                 % theoretical initial pressure when delta z is 0
  F = 2*pi*R*st*sin(con_angle)-pi*R^2* P0;   % the force need to hold top plate

  % 2. Given the distance between the needle and the board, dispensed fluid mass, calculate the
       critical shape of the bridge,which meets the Laplace's equation and boundary conditions.

  Dispen_mass =8/1000/1000                     % dispensed mass is 8 mg, changeable
  initial_V = 1.0e9*Dispen_mass/den          % the volume of the dispensed fluid.mm^3
  pause
  init_hdot1 = tan(con_angle)                % initial H dot
  Tfinal =2.000/1000;                          % Model simulation final time,s, changeable
  [t,x,y] = sim('bridge_model',Tfinal);      % simulation
  subplot(311), plot (t*1000,y(:,2)*1000,'k-');% Draw the interface
     hold on;
     Total_volume_1 = y(end,1)*1.0e9

  % 2.1 If the Total_volume at the initial angle is not the same as initial_V, then search as
        changing the initial contact angle
```

```
    if (Total_volume_1> 1.0100* initial_V); %Volume upper tolerance is 1% of the initial Volume
         disp('Total_volume_1 is bigger than initial_V');
         while Total_volume_1 > 1.0100*initial_V
            con_angle = con_angle + unit_angel           % change initial contact angle
             init_hdot1 = tan(con_angle);                % initial H dot
              if(init_hdot1 > 0);
              stop
             else
             [t,x,y] = sim('bridge_model', Tfinal);       % simulation
             Total_volume_1 = y(end,1)*1.0e9              % calculate volume
             clf
             subplot(311), plot (t*1000,y(:,2)*1000,'k-'); % Draw the interface
             hold on;
             end

         end

      elseif (Total_volume_1 < 0.9900*initial_V)    % Volume lower tolerance is 1% of initial_V
              display('Total_volume_1 is less than initial_V');
        while Total_volume_1 < 0.9900*initial_V
            con_angle = con_angle - unit_angel
             init_hdot1 = tan(con_angle);                  % initial H dot
             if (init_hdot1 > 0 );
                stop
             else
                  [t,x,y] = sim('bridge_model', Tfinal);      % liquid bridge shape simulation
                  Total_volume_1 = y(end,1)*1.0e9
                  clf
                  subplot(311), plot (t*1000,y(:,2)*1000,'k-');% Draw the interface
                  hold on;

             end
         end

      else
      disp('☺ ☺ Haha, the initial angle is right angle matching to intial volume');
    end

    Volume_board =y(end,4)*1.0e9
    Needle_volume = y(end,7)*1.0e9
    Length_equal_R0 = y(end,8)*1.0e3    % mm,
    Equal_R0_volume = y(end,5)*1.0e9
    Mini_R = y(end,6)*1.0e3
    interface_hdot = y(end,3);
    angle1 = atan(interface_hdot)*180/pi
  grid;  ylabel ('Critical shape');
  axis ([0 2.65 0 3.0]);

%The End
```